Published in final edited form as:

Mucosal Immunol. 2024 June ; 17(3): 431–449. doi:10.1016/j.mucimm.2023.12.001.

Metabolic fitness of IgA⁺ plasma cells in the gut requires DOCK8

Biyan Zhang[1,2,3,†], **Shuting Chen**[2,†], **Xiangyun Yin**[2], **Caleb D. McBride**[4], **Jake A. Gertie**[1,2], **Marina Yurieva**[5], **Agata A. Bielecka**[2,6], **Brian Hoffmann**[7], **J. Travis Hinson**[5,8], **Jessica Grassmann**[5], **Lan Xu**[1,2], **Emily R. Siniscalco**[1,2], **Arielle Soldatenko**[1,2], **Laura Hoyt**[1,2], **Julie Joseph**[1,9], **Elizabeth B. Norton**[10], **Gowthaman Uthaman**[1,2,11], **Noah W. Palm**[2], **Elise Liu**[1,2,12], **Stephanie C. Eisenbarth**[1,2,4,13], **Adam Williams**[4,5,13]

[1]Department of Laboratory Medicine, USA.

[2]Department of Immunobiology, Yale University School of Medicine, New Haven, CT 06520, USA.

[3]Singapore Immunology Network (SIgN), Agency for Science, Technology, and Research (A*STAR), 8A Biomedical Grove, Immunos, Singapore 138648, Singapore.

[4]The Department Medicine, Division of Allergy and Immunology, Northwestern University Feinberg School of Medicine, Chicago, IL 60611, USA.

[5]The Jackson Laboratory for Genomic Medicine, Farmington, CT 06030, USA.

[6]Department of Microbial Immunoregulation, Helmholtz Center for Infection Research, 38124 Braunschweig, Germany.

[7]Mass Spectrometry and Protein Chemistry, The Jackson Laboratory for Genomic Medicine, Bar Harbor, ME 04609, USA.

[8]Cardiology center, Department of Medicine, UConn Health, Farmington, CT, USA.

[9]Department of Microbiology and Immunology, Drexel University College of Medicine, Philadelphia, PA 19102, USA.

[10]Department of Microbiology & Immunology, Tulane University School of Medicine, New Orleans, LA 70112, USA.

[11]Department of Pathology, University of Massachusetts Medical School, Worcester, MA 01655, USA.

[12]Section of Rheumatology, Allergy & Immunology, Yale University School of Medicine, New Haven, CT 06520, USA.

stephanie.eisenbarth@northwestern.edu (S. C. Eisenbarth); adam.williams@northwestern.edu (A. Williams).

[†]These authors contributed equally.

AUTHOR CONTRIBUTIONS

B.Z., S.C., X.Y., A.W., and S.C.E. conceived and designed the project. B.Z., S.C., X.Y., C.D.M., J.A.G., A.A.B., B.H., J.G., L.X., E.S., A.S., L. H., J.J., G.U., E.L., and A.W. performed experiments and analyzed the data. M.Y. analyzed data and generated figures. J.T.H., N.W.P., and E.B.N. provided advice and essential tools. B.Z., S.C., B.H., A. W., and S.C.E. generated figures and wrote the paper, and all authors reviewed and approved the final version of this manuscript to be published.

APPENDIX A. SUPPLEMENTARY MATERIAL

Supplementary data to this article can be found online at https://doi.org/10.1016/j.mucimm.2023.12.001.

Conflict of Interest Statement

No conflict.

[13]Center for Human Immunobiology, Northwestern University Feinberg School of Medicine, Chicago, IL, USA.

Abstract

Dedicator of cytokinesis 8 (DOCK8) mutations lead to a primary immunodeficiency associated with recurrent gastrointestinal infections and poor antibody responses but, paradoxically, heightened IgE to food antigens, suggesting that DOCK8 is central to immune homeostasis in the gut. Using *Dock8*-deficient mice, we found that DOCK8 was necessary for mucosal IgA production to multiple T cell-dependent antigens, including peanut and cholera toxin. Yet DOCK8 was not necessary in T cells for this phenotype. Instead, B cell-intrinsic DOCK8 was required for maintenance of antigen-specific IgA-secreting plasma cells (PCs) in the gut laminapropria. Unexpectedly, DOCK8 was not required for early B cell activation, migration, or IgA class switching. An unbiased interactome screen revealed novel protein partners involved in metabolism and apoptosis. *Dock8*-deficient IgA^+ B cells had impaired cellular respiration and failed to engage glycolysis appropriately. These results demonstrate that maintenance of the IgA^+ PC compartment requires DOCK8 and suggest that gut IgA^+ PCs have unique metabolic requirements for long-term survival in the lamina propria.

Graphical Abstract

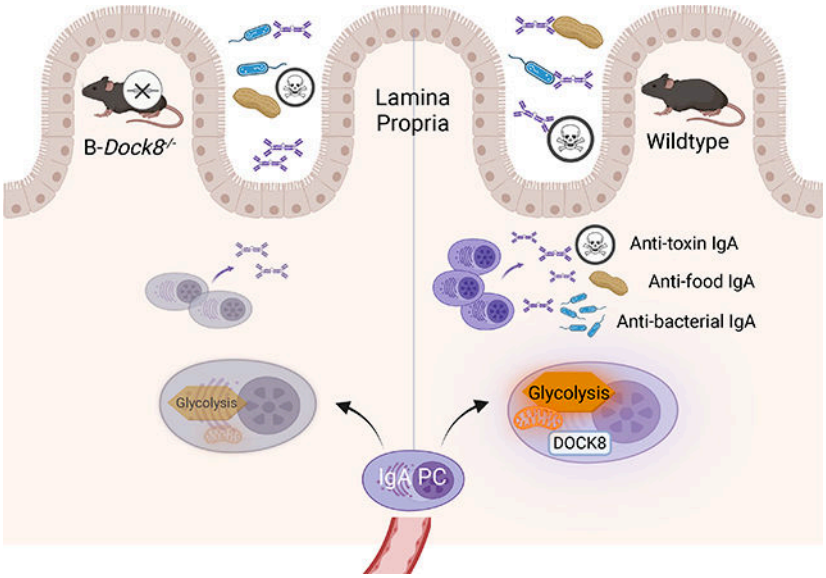

INTRODUCTION

The gut is a unique tissue that maintains tolerance to commensal microbes as well as foreign antigens from the diet while simultaneously defending against invading pathogens. Dysregulation of this balance can lead to infection, inflammatory bowel disease, or food allergy. Physical barriers such as a thick mucus layer, antimicrobial proteins, and mucosal antibodies, in particular IgA, defend against pathogenic bacteria while retaining symbiotic commensal bacteria[1–3]. Apart from regulating bacteria, gut IgA is important in neutralizing toxins and has been hypothesized to also exclude food[4–7]. Yet fundamental unanswered

questions exist about how IgA is induced and its function[8]. We discovered that most children and adults make allergen-specific IgA in the gut, but our work questions whether anti-food allergen IgA is a marker of tolerance[9]. Therefore, we are working to identify the cellular mechanisms of food-specific IgA induction.

IgA is present both in the blood and at mucosal sites; the primary site of production is in the gut lamina propria (LP) by plasma cells (PCs). Many cellular and molecular aspects of IgA production have been established primarily by evaluating the response to bacteria or toxins[8,10]. Broadly, IgA can be made in a T cell-dependent or T cell-independent manner and is induced in the mesenteric lymph nodes (MLN), Peyer's patches (PP), and isolated lymphoid follicles. IgA responses to T cell-dependent antigens, such as food allergens, cholera toxin (CT), and keyhole limpet hemocyanin, require CD40 activation on B cells[11,12], while T cell-independent IgA switching can occur in response to a proliferation-inducing ligand (APRIL) and B cell-activating factor (BAFF)[13–15]. The contribution of T cells to the majority of anti-commensal IgA in the gut remains debated[8]. Transforming growth factor β (TGF-β) is the major cytokine for IgA class switching as isolated deletion of TGF-β receptor II (TGF-βRII) on B cells significantly impairs CT-specific serum and secretory gut IgA[16,17]. *In vitro*, interleukin (IL)-2, IL-4, IL-5, IL-6, IL-10, and IL-21, as well as retinoic acid (RA), have all been demonstrated to contribute to IgA switching together with TGF-β[10].

The particular susceptibility of patients with *DOCK8* mutations to infections of the gastrointestinal tract and severe food allergies led us to test whether DOCK8 has a unique role in promoting gut IgA. DOCK8 is an atypical guanine nucleotide exchange factor (GEF) belonging to the DOCK180 superfamily that plays a fundamental role in many immunoregulatory processes[18,19]. DOCK8 is involved in a myriad of biological functions such as cellular migration, signaling, and adhesion, in particular in cells of the immune system[20–27]. DOCK8 is also important for maintaining long-lived systemic antibody responses, although exactly how is not clear; mechanisms that have been proposed include promoting B cell receptor (BCR) signaling through Wiskott-Aldrich syndrome protein (WASP) and CD19, stabilizing B cell immunological synapses, and enhancing TLR9 signaling through MYD88[28–30]. Although Dock8 deficiency has been associated with defective long-lived humoral responses in mice and poor vaccine responses in humans, most studies focus on systemic antibody responses, and less is known about the effect of DOCK8 deficiency on mucosal antibodies[20,21,28–34]. In patients, DOCK8 deficiency leads to variable serum IgA levels ranging from high, normal, or low as compared to healthy individuals; however, stool IgA levels have not been reported[20,21,32–34]. As these patients often take antibiotics for recurrent bacterial infections, this poses a potential barrier to the interpretation of data from the study of stool IgA. A recent report of *Dock8*-deficient mice revealed impaired microfold (M) cell development, which was associated with impaired fecal IgA[31]. Whether this impaired ability to sample luminal contents results in the observed susceptibility of patients with *DOCK8* mutations to gut infection and food allergy or instead is due to an immune cell-intrinsic defect is an open question.

Using cell-specific *Dock8*-deficient mice, we examined the role of DOCK8 on the gut humoral immune response to foreign antigens including toxins, bacteria, and food allergens.

We found that DOCK8 is indispensable for gut IgA to toxins, food, and certain bacteria. Specific deletion of *Dock8* in B cells (B-*Dock8*$^{-/-}$), but not T cells, recapitulated the loss of IgA. Yet, by evaluating antigen-specific B cells in the MLN, PP, and bone marrow (BM), we found that priming and differentiation of IgA^{+} B cells into antibody-secreting cells were intact. Instead, only antigen-specific IgA^{+} PCs in the LP were defective. Despite known involvement of DOCK8 in cell migration and STAT3 signaling, both of which could contribute to loss of antigen-specific IgA^{+} PCs in the LP, *Dock8*-deficient B cells demonstrated normal migration and normal STAT3-phosphorylation upon IL-21 simulation. Using TurboID to characterize the protein interactome of DOCK8, we found enrichment of proteins involved in regulation of cytoskeleton remodeling, signaling, and GTPases. Surprisingly, DOCK8 was also found to interact with proteins involved in apoptosis, autophagy, and cell metabolism. *In vitro* studies using CD40L-activated *Dock8*-deficient IgA-switched B cells confirmed impaired respiration, supporting a previously unknown role of DOCK8 in regulating the survival of antigen-specific IgA^{+} PCs through the regulation of metabolic pathways. These results suggest that DOCK8 might enable PC adaptation to the variable metabolic environment described in the gut LP with feeding[35]. This new knowledge could help explain the susceptibility of *DOCK8*-deficient patients to gastrointestinal infections as well as shed light on new aspects of PC maintenance in the gut through metabolic pathways.

RESULTS

Dock8-deficient mice have impaired gut IgA production

To study the effect of *Dock8* deficiency on mucosal antibodies, we measured total IgA, IgG, IgM, and IgE in the stool of *Dock8*-deficient (*Dock8*$^{-/-}$) mice at steady state. Comparison of stool antibody isotypes in *Dock8*$^{-/-}$ and cohoused *Dock8*$^{+/+}$ and *Dock8*$^{+/-}$ littermate control mice revealed a significant reduction in free fecal IgA in mice lacking DOCK8, but not IgG, IgG sub-types, or IgM (Fig. 1A, Fig S1A–B). We also found a consistent IgA defect in *Dock8*$^{-/-}$ mice irrespective of gender (S1A). In line with previous work, IgA was the predominant antibody isotype in the stool of wild-type (WT) C57BL/6 mice, followed by IgG and IgM, while IgE was below the detection limit of our assay in the stool of all mice tested at steady state (Fig. 1A, Fig. S1C)[12]. Consistent with stool antibody data, we observed a decrease in sera IgA from *Dock8*$^{-/-}$ mice (Fig. S1D), which likely reflects the loss of IgA from the gut[36–38]. Consistent with our previous work, complete *Dock8*-deficient mice had normal, low levels of total IgE in the serum (Fig. S1D)[39].

As a large amount of gut IgA is directed against commensal bacteria and is relevant for shaping the diversity and composition of the microbiome[40,41], we asked whether the loss of IgA in the stool of *Dock8*$^{-/-}$ mice altered gut microbial composition. Using flow cytometry, we assessed the frequency of IgA-coated bacteria in the stool samples as described by Palm and de Zoete et al.[42] (Fig. S2A). Analysis of total IgA-bound bacteria in *Dock8*$^{+/-}$ and *Dock8*$^{-/-}$ cohoused littermates revealed no difference in the frequency of IgA-coated bacteria (Fig. S2B). 16S rRNA sequencing data also revealed no major changes in the relative abundance of bacterial families between *Dock8*$^{+/-}$ and *Dock8*$^{-/-}$ cohoused littermates (Fig. S2C). However, LEfSe analyses revealed an increase in certain bacteria

including segmented-filamentous bacteria (SFB) in *Dock8*$^{-/-}$ mice as compared to littermate controls, consistent with observations by Kunimura et al. in a different *Dock8*-deficient mouse line (Fig. S2D)[31,43].

Given the expansion we observed in SFB in *Dock8*$^{-/-}$ mice and the reduced levels of gut IgA, we next evaluated the degree of IgA coating of gut bacteria from *Dock8*$^{-/-}$ and control littermate mice using "IgA-Seq"[42]. We compared beta diversity by performing principle coordinate analysis, which revealed an expected segregation of IgA^{+} bacteria from IgA^{-} and total (presorted) bacteria but did not further segregate samples by genotype (Fig. 1B). Representation of these data in a cladogram showed that IgA^{+} bacteria segregated from both the IgA^{-} and presort fractions, regardless of mouse genotype (Fig. 1C). Further assessment of the microbiome diversity using Chao1 indices, which denote bacterial species richness in both IgA^{+} and IgA^{-} stool fractions from *Dock8*$^{+/+}$, *Dock8*$^{+/-}$, and *Dock8*$^{-/-}$ also demonstrated no major changes in alpha diversity (Fig. S2E). To detect that more subtle differences in IgA to bacteria might exist, we used SFB isolated from monocolonized mice and incubated it with stool supernatants from Dock8$^{+/-}$ or Dock8$^{-/-}$ mice housed in our SFB^{+} facility. IgA flow revealed a small defect in SFB-specific IgA production (Fig. 1D), suggesting that production of specific IgA might be selectively impaired in *Dock8*-deficient mice.

Besides commensal bacteria, food antigens are another major source of foreign antigens in the gut. CT is one of the most commonly used gut mucosal adjuvants and induces high levels of IgA to food when co-administered[12]. To determine if *Dock8* deficiency affects IgA responses to food antigens, we immunized *Dock8*$^{+/-}$ mice and Dock8$^{-/-}$ littermate controls with peanut and CT. Gut peanut-specific IgA (PN IgA) was undetectable in immunized *Dock8*$^{-/-}$ mice (Fig. 1E). Heat-labile toxin (LT) from *E coli*. has been shown to be another effective mucosal adjuvant to induce antigen-specific IgA responses to protein antigens[44,45]. Using this alternative adjuvant, we immunized mice to peanut and found a similar decrease in stool peanut IgA in *Dock8*$^{-/-}$ mice (Fig. S1E). In addition to acting as an adjuvant, CT also induces a well-characterized T cell-dependent IgA response to itself[5,46]. As such, we measured IgA responses to CT (CT IgA) and found that it was completely abrogated in *Dock8*$^{-/-}$ mice (Fig. 1F). Collectively, *Dock8* deficiency did not result in a major alteration in IgA-regulated microbial diversity but did impair the production of IgA to select bacteria, bacterial toxins, and food antigens. These data suggest a restricted role of DOCK8 in gut IgA responses that require T cell help.

Loss of DOCK8 impairs IgA-mediated protection from CT

Both J chain and polymeric Ig receptor knockout mice have impaired protection against CT-induced diarrhea upon secondary exposure, predominantly affecting secreted IgA in the gut lumen that is important for protection[47,48]. To test if impaired production of CT IgA resulted in failed protection from toxin-induced diarrhea, we challenged mice with CT 10–14 days post immunization. Consistent with robust IgA production to CT following immunization in *Dock8*$^{+/-}$ but not *Dock8*$^{-/-}$ mice, only *Dock8*$^{+/-}$ mice were protected from diarrhea upon secondary challenge with CT (Fig. 2A–B). CT-immunized *Dock8*-deficient mice had increased intestinal weight due to fluid accumulation in the intestine, which was

comparable to unimmunized mice upon challenge with CT (Fig. 2C). As the difference in fluid accumulation in cecum was most evident, a significant increase in cecum weight was also observed in *Dock8*$^{-/-}$ mice (Fig. 2C). Therefore, DOCK8 is indispensable for the production of toxin neutralizing IgA in the gut.

Antigen-specific IgA production is independent of DOCK8 in T cells

Loss of DOCK8 in T cells has been associated with impaired differentiation and aberrant function in multiple T cell subsets, including T helper 17 (Th17), T follicular helper, and regulatory T cells (Treg)[27,39,49,50]. As these T cell subsets have been implicated in the promotion and regulation of gut IgA responses, we wanted to understand if loss of T cell-dependent IgA was due to intrinsic loss of DOCK8 in T cells[51,52]. Through isolation of *Dock8* deficiency to T cells using *Cd4*-Cre mice crossed to a floxed *Dock8* mouse we generated (previously described by Gowthaman et al.[39]), we found that stool IgA to peanut (Fig. 3A) was intact. As such, these data suggest that although DOCK8 might be particularly important for T cell-dependent IgA production, expression of *Dock8* in T cells is not necessary for the production of this IgA.

B cell-intrinsic *Dock8* deficiency impairs gut IgA production to food antigens

Several groups had previously demonstrated that *Dock8*-deficient B cells have impaired long-lived systemic antibody responses as a result of defects in immunological synapse formation as well as BCR and TLR9 signaling[28–30]. Therefore, we hypothesized that B cell-intrinsic defects might be responsible for failed T cell-dependent IgA responses in *Dock8*$^{-/-}$ mice. Using mixed chimeras reconstituted with *Dock8*$^{-/-}$ and muMt$^{-/-}$ (*Ighm*$^{-/-}$) donor BM at a 1:1 ratio, we isolated *Dock8* deficiency to B cells and found impaired gut IgA production to peanut (Fig. 3B).

We generated conditional deletion of *Dock8* in B cells by crossing *Cd23*-Cre mice to *Dock8* floxed mice (B-Dock8$^{-/-}$). *Cd23*-Cre is used for conditional deletion of genes in late B cell lymphopoiesis as the Cre is active in a subpopulation of immature B cells, all transitional, marginal zone, and follicular B cells[53]. Immunoblot of purified splenic follicular B cells revealed a loss of DOCK8 protein in B-Dock8$^{-/-}$ but not control mice, indicating efficient deletion of DOCK8 (Fig. S3A). Characterization of total and follicular splenic B cell frequencies and numbers in B-Dock8$^{-/-}$ mice revealed largely normal B cell development (Fig. S3B–C). However, B-Dock8$^{-/-}$ mice had impaired marginal zone B cells (Fig. S3C) consistent with previous reports in total *Dock8*$^{-/-}$ mice[30,54]. Unlike human marginal zone B cells, there is abundant literature that murine marginal zone B cells are restricted to the spleen, and therefore, it is unlikely that the loss of marginal zone B cells contributes to the loss of IgA to T cell-dependent antigens in the gut in the *Dock8*$^{-/-}$ mice[55].

Similar to the chimeras, B-Dock8$^{-/-}$ mice had impaired stool peanut-specific (Fig. 3C) and CT-specific IgA responses (Fig. 3D), albeit not to the same extent as total *Dock8*$^{-/-}$ mice (Fig. 1). In contrast to complete *Dock8*$^{-/-}$ mice, total stool IgA levels in B-Dock8$^{-/-}$ mice were comparable to littermate controls (Fig. 3E). This is supported by normal levels of total IgA-secreting cells in the small intestine lamina propria (SiLP) in B-Dock8$^{-/-}$ measured by enzyme-linked immunospot (ELISpot) assay (Fig. 3F). Given the importance of PPs for IgA

in the gut[56] and prior work demonstrating a loss of PPs in *Dock8*$^{-/-}$ mice due to defective M cell development[31] we compared PP cellularity between *Dock8*$^{-/-}$ and B-Dock8$^{-/-}$ mice. Indeed, complete loss of DOCK8 resulted in hypoplastic PP (Fig. S3D), whereas isolated loss of DOCK8 in B cells did not alter cellularity of the PPs (Fig. S3E). Therefore, multiple cellular defects in total *Dock8*$^{-/-}$ mice result in loss of the majority of gut IgA production. In contrast, specific loss of DOCK8 in just B cells led to impaired IgA responses to multiple antigenic targets. To understand if loss of DOCK8 in B cells differentially affects high versus low affinity IgA, we immunized B-Dock8$^{-/-}$ mice and littermate controls with the haptenated antigen NP-OVA with CT. B-Dock8$^{-/-}$ mice showed reductions in both moderate-affinity and high-affinity NP-specific IgA (Fig. 3G). We therefore focused on understanding the role of DOCK8 in B cells in the production of food-specific IgA.

B cell-intrinsic *Dock8* deficiency does not alter B cell migration, gut homing, or MLN and PP architecture

DOCK8 is important in the regulation of the actin network and had been previously shown to impair CX3CR1^{+} mononuclear phagocytes, dendritic cell, and CD8 T cell migration[22–26]. This led us to hypothesize that impaired gut IgA responses to T cell-dependent antigens could be due to 1) impaired migration of B cells to MLN and PP, which are the major inductive sites for T cell-dependent IgA production or 2) impaired migration of antigen-specific B cells to the SiLP, which is the effector site for antigen-specific IgA^{+} PCs[57].

Comparison of total IgA^{+} B cell frequencies in MLN and PP of B-Dock8$^{-/-}$ and littermate controls revealed no significant differences (Fig. S3F), indicating that B cells could migrate successfully to these sites. Impaired antigen-specific IgA responses could be due to improper localization of B cells within MLNs and PPs. For example, CCR6 expression is necessary for proper positioning of B cells in the subepithelial dome for CT-specific IgA responses[56]. To assess this, we used immunofluorescent microscopy, which revealed intact immunologic structures and organization of both the PP and MLN in B-Dock8$^{-/-}$ mice as compared with cohoused littermates (Fig. 4A–B): intact IgD^{+} naïve B cell zones, IgD^{-} germinal centers (GCs), T cell zones, and CD11c^{+} dendritic cells distributed within the subepithelial dome and T cell zones. IgA^{+} B cells were also found inside and outside GCs. Altogether, these data suggest that IgA^{+} B cells lacking DOCK8 can appropriately populate MLN and PP at steady state.

Gut homing of B cells to SiLP is primarily mediated by the chemokine receptor CCR9[58]. In addition, the interaction between α4β7 and mucosal vascular addressin, MAdCAM-1, is necessary for cell trafficking to mucosal sites[59]. To test whether *Dock8*-deficient IgA^{+} cells have a defect in homing to mucosal sites in particular, SiLP, we compared the expression of α4β7 and CCR9 on IgA^{+} B cells and found that the frequency of CCR9 and α4β7 double positive cells in IgA^{+} B cell population is comparable in the PP and MLN of control and B-Dock8$^{-/-}$ mice (Fig. 4C, D). We further tested the ability of IgA^{+} cells isolated from MLN to respond to the CCR9 ligand, CCL25, using transwell migration assays. A similar percentage of control and *Dock8*-deficient CCR9^{+} IgA^{+} B cells migrated to CCL25 (Fig. 4E), indicating normal CCL25 chemotaxis in *Dock8*-deficient IgA^{+} B cells. Lastly, as T cells and myeloid cells lacking DOCK8 have been shown to have normal chemotaxis but

undergo cytothripsis during migration in three-dimensional (3D) collagen gel matrix[22,26], we tested the ability of *in vitro* differentiated IgA$^+$ B cells to migrate towards CCL25 in 3D collagen gels. We found that *Dock8*-deficient IgA$^+$ B cells migrated normally in terms of distance and without evidence of cytothripsis (Fig. 4F). Altogether, these data demonstrated that *Dock8*-deficient IgA$^+$ B cells can express gut-homing chemokine receptors as well as respond and migrate towards gut-homing chemokine signals in 2D and 3D matrices. This suggests that loss of DOCK8 in B cells does not impair their ability to migrate and is unlikely to contribute to the impairment in IgA production.

B cell-intrinsic *Dock8* deficiency results in decreased antigen-specific IgA$^+$ PCs in LP but not PP, MLN, or BM

To identify how B cell-intrinsic loss of DOCK8 impaired T cell-dependent gut IgA, we examined the various B cell populations in the MLN, PP, and SiLP that contribute to IgA production post immunization with T cell-dependent antigens, peanut, and CT, in B-Dock8$^{-/-}$ mice. Given our previous work demonstrating that T follicular helper cells (Tfh)-knockout mice, which also lose GCs, develop normal peanut-specific IgA under the same immunization conditions[12] and the observable GC staining in Fig. 4A–B, we did not anticipate that a loss of IgA$^+$ B cells in GCs would explain our phenotype, but we checked for this phase of B cell activation in the MLNs and PPs using flow cytometry because overall GC magnitude was reduced in B-Dock8$^{-/-}$ mice. Indeed, the frequency of IgG1$^+$ but not IgA$^+$ GC B cells was significantly reduced in both MLNs and PPs (Fig. S4A–D). Using CD138 as a marker of early plasmablasts (PB) and later PC differentiation, we observed normal levels of IgA$^+$ PB/PC in the MLN and a slight but not statistically significant decrease of IgA$^+$ PB/PC in the PPs of B-Dock8$^{-/-}$ mice (Fig. S4E–F). However, this mild defect did not result in a reduction of total IgA$^+$ PB/PC in SiLP of B-Dock8$^{-/-}$ mice (Fig. S4G). These findings likely explain why the total stool IgA in B-Dock8$^{-/-}$ mice was normal (Fig. 3E–F).

We had examined total B cell populations in both MLNs and PPs post immunization, but the majority of gut IgA is likely against bacteria with only a small proportion of IgA$^+$ B cells specific to our immunogen. Using ELISpot assays, we found a significant reduction in both CT IgA and peanut IgA ASCs in the SiLP of B-Dock8$^{-/-}$ mice as compared to their cohoused littermates (Fig. 5A). However, this reduction was not seen in the MLN or PP (Fig. 5B–C), indicating that early stages of B cell differentiation into CT and peanut IgA-secreting PB are intact, but PB/ PC fails to generate or persist in the SiLP. Examination of another PC niche, the BM, revealed normal numbers of peanut-specific IgA-secreting cells (Fig. 5D). Therefore, generation of antigen-specific IgA$^+$ PCs is intact in the absence of DOCK8 but fail to be maintained selectively in the LP. Recent data comparing IgA$^+$ PCs in different niches in fact demonstrated that while BM and LP IgA$^+$ PCs have related clonality, suggesting shared origins, the two populations express tissue-specific gene signatures[38]. Therefore, these data support a model in which the requirements to maintain antigen-specific PCs within the BM and siLP are different.

Using another method to characterize antigen-specific B cells in the MLNs and PPs, we immunized B-Dock8$^{-/-}$ mice with the T cell-dependent antigen NP-OVA and CT and

examined the B cell subsets in the MLNs and PPs by flow cytometry. Consistent with ELISpot results, detection of NP-specific $CD138^+$ IgA B cells by flow cytometry identified an impairment in the SiLP, but not PPs and MLNs (Fig. 5E–G). To understand if the loss of NP-specific $CD138^+$ IgA cells is PB or PC, we used Ki67 to distinguish the two populations. Ki67 is a marker of proliferating cells and can be used to differentiate actively-dividing PB from long-lived, non-proliferating PC[60,61]. Comparison of the percent of NP-specific IgA^+ B cells that were $Ki67^+$ revealed a slight but not statistically significant increase PB in SiLP of B-$Dock8^{-/-}$ mice (Fig. S4H). As MLN and PP are known to contain precursors for IgA^+ PC found in the LP[61–63], these data suggest that loss of DOCK8 in B cells does not impair priming, IgA switching, or PB differentiation but instead likely impairs terminal differentiation or maintenance of PCs specifically within the SiLP.

DOCK8 in B cells is not required for B cell activation, IgA class switching, or differentiation into antibody-secreting cells

To further understand the underlying molecular mechanisms in the requirement for DOCK8 in the persistence of PCs in the SiLP, we examined several key molecules and pathways important for PC differentiation to T cell-dependent antigens. As loss of DOCK8 in B cells had been demonstrated to impair BCR signaling due to reduced *Cd19* expression[29], we checked surface CD19 protein expression in our model and found them comparable between *Dock8*-sufficient and *Dock8*-deficient B cells (Fig. S5A). DOCK8 promotes the phosphorylation and nuclear translocation of STAT3 in T cells[64]. STAT3 is an important transcription factor downstream of three cytokines involved in PC development, IL-21, IL-6, and IL-10[65–68]. In particular, IL-21 supports GC and PC differentiation synergistically with CD40L[69]. In the gut, IL-21 has also been shown to boost IgA production by intestinal B cells[70], and *Il21r*-deficient mice have expanded SFB, lower fecal IgA, and reduced IgA^+ PCs in PP and SiLP at steady state[71]. Therefore, we hypothesized that *Dock8* deficiency in B cells could result in defective STAT3 activation and thereby reduced terminal PC differentiation in the LP. Since CD40 can act synergistically with IL-21 to promote PC differentiation, we first examine the levels of CD40 on *Dock8*-deficient B cells and found it to be similar as WT controls (Fig. S5B). Next, we tested STAT3 phosphorylation at Tyrosine 705 in response to IL-21 and found that STAT3 signaling downstream of IL-21 activation was intact (Fig. S5C).

Although there is general consensus regarding key cytokines necessary for IgA switching, the conditions necessary for generation of robust IgA^+ PCs *in vitro* have been elusive, and most methods result in limited generation of IgA-secreting cells[10]. As DCs have been shown to be involved in IgA switching *in vivo* in PPs, we established a system of DC-B cell co-culture with *in vitro* generated BM derived DCs and naïve B cells isolated from PP or spleen[56,58]. To model T cell activation in the gut, we activated the B cells with CD40L and α-IgM together with polarizing cytokines, TGFβ, as well as RA in the presence of BMDCs. Using this system, we attained a large number of IgA-switched cells, which could be used to understand the molecular requirements of DOCK8 for IgA^+ PC generation (Fig. S5D–E). Using both naïve B cells isolated from the spleen (Fig. S5D) or PP (Fig. S5E), we found that, consistent with our *in vivo* data, IgA class switching was intact.

DOCK8 interacts with molecules associated with cell metabolism in IgA$^+$ B cells and is necessary for normal cellular respiration

To better understand DOCK8 function, we sought to map the DOCK8 interactome in IgA$^+$ B cells. For this, we utilized TurboID, which is a proximity-dependent tagging method using a modified version of *E. coli* BirA that exhibits promiscuous lysine biotinylation within a 10 nm radius of expression[72]. Using CRISPR/Cas9, we generated a mouse strain in which TurboID was inserted in-frame into the last coding exon of the *Dock8* gene, generating a DOCK8-TurboID fusion protein expressed from the endogenous locus (Fig. S6A). Addition of 50 mM biotin to *in vitro* generated IgA$^+$ B cell cultures provided strong biotinylation signal in lysates obtained from DOCK8-TurboID cells as compared to biotin-pulsed WT control cells (Fig. S6B).

To identify DOCK8 proximity partners, we subjected lysates from biotin-pulsed DOCK8-TurboID and control non-TurboID IgA$^+$ B cells generated *in vitro* from PP cells to streptavidin affinity purification followed by tandem mass spectrometry (Table S1). Analysis of DOCK8-TurboID versus non-TurboID samples identified enrichment of 321 DOCK8 proximity partners (log2 fold change ≥1 and false discovery ≤0.05; Fig. S6C–D; Table S1). Gene Ontology (GO) and Ingenuity Pathway Analysis (IPA) analysis revealed many proteins from pathways known to involve DOCK8 including GTPase regulation and signaling and cytoskeleton remodeling (Fig. 6A and S6E). We also identified proteins in pathways not previously associated with DOCK8 including apoptosis, autophagy, and metabolism (Fig. 6A). This suggests that DOCK8 may have diverse cellular functions.

Recently, the importance of metabolic pathways in regulating B cell effector functions has been identified[73]. In particular, shifts in metabolic pathways used in terminally differentiated PCs enable antibody secretion and survival[74]. Naïve B cells and IgA$^+$ PC in the gut use distinct metabolic pathways, with IgA$^+$ PC relying on both tricarbolylic acid cycle (TCA) and glycolysis for ATP generation while the naïve B cells from PP predominantly using TCA cycle[75]. Our TurboID data revealed that DOCK8 potentially interacts with several proteins in the glycolytic pathway such as Phosphofructokinase, Liver Type (PFKL), TP53 Induced Glycolysis Regulatory Phosphatase (TIGAR), and Pyruvate Kinase M1/2 (PKM) (Fig. 6A and S6D). PKM is an important rate-limited enzyme in the generation of pyruvate, which is used to support respiration and promote survival of long-lived PCs during states of metabolic stress[74]. Therefore, we aimed to validate the molecular interaction of DOCK8 and PKM. Proximity ligation assays (PLA) allow *in situ* detection of endogenous protein-protein interactions with high specificity and sensitivity at single-molecule resolution. As a reliable anti-mouse DOCK8 antibody is not available, we took advantage of the single HA tag included in the DOCK8-TurboID fusion protein. Using PLA of *in vitro* generated DOCK8-TurboID IgA$^+$ B cells, we confirmed the interaction between DOCK8 and PKM, validating our TurboID mass spectrometry data (Fig. 6B). B cells lacking the HA tag, and therefore should not be recognized by one of the antibody pairs, confirmed the specificity of the assay (Fig. 6B left).

Recent work has shown that metabolic differences rather than major transcriptional differences differentiate long-lived from short-lived PCs in other compartments[73]. Therefore, we hypothesized that loss of DOCK8 might impair glucose and energy metabolism in

IgA$^+$ PCs. To test this hypothesis, we quantified oxygen consumption rates and the proton efflux rate (glycoPER), which estimates the amount of lactate production produced from glycolysis. *Dock8*-deficient IgA$^+$ B cells had a reduction in both basal mitochondrial oxygen consumption and glycolysis (Fig. 6C). Upon pharmacological inhibition of mitochondrial respiration with rotenone and antimycin, *Dock8*-deficient cells failed to compensate with an increase in glycolytic rates (Fig. 6C). These data suggest that DOCK8 is crucial for basal ATP production and engaging reserve pathways to compensate when respiration is impaired, both of which are required for PC longevity in particular in the gut given the cyclic availability of nutrients[35,74]. Thus, the antigen-specific IgA$^+$ PC compartment in the siLP is compromised without DOCK8 likely secondary toimpaired metabolic fitness, potentially due to a unique metabolic environment present in the siLP (Graphical Abstract).

DISCUSSION

Understanding the B cell extrinsic and intrinsic factors that drive the differentiation and maintenance of gut IgA responses is important to our understanding of tolerance and, conversely, loss of tolerance in states such as inflammatory bowel disease and possibly food allergy. Although gut IgA to toxins and bacteria is central to protection and homeostasis, the actual role of IgA to food antigens remains enigmatic[9]; this is in part due to the lack of knowledge about how food-specific IgA is induced. We used a mouse model of *Dock8*-deficiency to identify cellular mechanisms of food-specific IgA induction in the gut.

Much is known about the role of DOCK8 in mediating systemic humoral responses, but its role in mucosal antibody production has not been extensively studied[28–31]. We discovered that DOCK8 is necessary for T cell-dependent IgA responses to the bacterial toxin CT and the dietary antigen, peanut (Graphical Abstract). In addition, IgA to SFB was impaired; however, gross levels of IgA to commensal bacteria were unaffected by *Dock8*-deficiency. This observation is congruent with data showing normal IgA binding to most commensal bacteria except a few taxa such as SFB, *Mucispirillum*, and *Helicobacter* in *Tcr*$\beta^{-/-}\gamma^{-/-}$ mice[42,76]. The control of SFB was previously found to depend on activation-induced cytidine deaminase (AID) and thought to require T cell help[77]. Indeed, similar to 16S rRNA sequencing data generated by Kunimura et al. (2019), our data revealed an expansion of SFB despite using a different model of *Dock8*$^{-/-}$ mice[31]. Taken together, these data suggest that DOCK8 is specifically required during a T cell instructed IgA response; however, numerous fundamental questions remain in the IgA field, in particular around the nature of T cell help for IgA, so this pattern of IgA loss in mice lacking *Dock8* should be interpreted cautiously[8].

A previous study had demonstrated an association between the loss of PPs in total *Dock8*$^{-/-}$ mice and impaired IgA responses resulting from developmental defects in M cells[31]. Consistent with these findings, we observed small PPs in complete *Dock8*$^{-/-}$ mice. Therefore, we generated a mouse model with conditional deletion of *Dock8* to understand whether a T cell- or B cell-intrinsic loss of DOCK8 is responsible for the loss of IgA responses without grossly impairing PP structures. Although *Dock8*-deficiency has been found to impair Treg cell function[27,50] and Th17 cell differentiation[64], and these two populations have also been implicated in driving IgA responses[51,52,78,79], loss of DOCK8 in T cells did not impair IgA responses to CT and peanut. In contrast, loss of specific, but

not total, IgA was associated with B cell-intrinsic *Dock8*-deficiency. This is consistent with findings in mice lacking CD40/CD40L in which specific IgA is impaired but total gut IgA is relatively normal[11,12]. As such, we believe that the total stool IgA defect in complete *Dock8*-deficient mice is caused by a B cell-extrinsic defect, likely attributed to a decrease in PP numbers and size, but the loss of antigen-specific IgA in *Dock8*$^{-/-}$ mice is contributed by a B cell-intrinsic defect.

Previously, loss of DOCK8 in B cells had been demonstrated to impair BCR signaling due to reduced *Cd19* expression[29]; however, we did not observe a significant decrease in surface CD19 on B cells from B-Dock8$^{-/-}$ mice. Another study of *Dock8*-deficiency in B cells revealed impaired long-lived systemic antibody responses, attributed to a defect in formation of immunological synapse, thereby crippling late GC responses[30]. However, the effect of this on mucosal IgA response was not explored. In our study, we also observed a reduction in frequencies of IgG1^{+} GC B cells in both MLNs and PPs, but frequencies of IgA^{+} GC B cells were unimpaired in *Dock8*-deficient mice. These results are consistent with our previous study demonstrating that induction of T cell-dependent mucosal IgA, but not IgG1, can occur in the absence of GCs[12]. Lastly, DOCK8 has been implicated in TLR9 signaling[28], and although *Tlr9*-deficient mice have impaired serum IgA upon immunization with peanut+CT, they also have reduced numbers of PPs[31,80]. Indeed a study showing normal IgG after intranasal immunization of *Myd88*$^{-/-}$ mice with CT and antigen could suggest that mucosal IgA induced by CT might not require TLR9 signaling[81]. Characterization of antigen-specific B cells in MLNs and PPs of B-Dock8$^{-/-}$ mice revealed normal numbers of peanut-specific IgA-secreting cells in MLN and PP, yet they were significantly reduced in LP. Consistent with normal B cell differentiation, STAT3-dependent IL-21 signaling was also intact. These data indicated that induction of antigen-specific IgA-secreting cells does not require DOCK8 and implicated impaired IgA^{+} PC migration or maintenance in the LP. As DOCK8 regulates migration of multiple cells of the immune system, we tested whether DOCK8 was necessary for IgA^{+} B cell migration. The expression of the gut-homing receptors CCR9 and $\alpha_4\beta_7$[58,59,82] was normal in *Dock8*-deficient IgA^{+} B cells, and migration *in vitro* to CCL25 was intact. Although we used systems that mimic migration through tissues, it is still possible that *in vivo* migration requires DOCK8. However, we concluded that the contribution of any migration/homing defect would be minor given these results, the normal cellular architecture of the MLN and PPs, and normal IgA ASCs in the BM; therefore, we explored alternative mechanisms explaining the diminished gut PC frequencies.

We performed an unbiased screen of DOCK8 protein interactions in IgA^{+} B cells generated from PP B cells using a TurboID-based proximity labeling assay. This screen identified proteins involved in actin cytoskeleton remodeling, which are known functions of DOCK8. Unexpectedly, we discovered that DOCK8 also potentially interacts with proteins involved in metabolism and apoptosis. Using an imaging-based *in situ* PLA, we validated that DOCK8 interacts with PKM, which regulates the final rate-limiting step of glycolysis. Therefore, we postulated that DOCK8 promotes the survival of IgA^{+} PCs by regulating metabolic fitness since glucose metabolism had been found to be essential for PC survival and antibody secretion systemically[73]. Long-lived PCs have greater spare respiratory capacity than short-lived PC as they can divert glucose into the glycolytic pathway for

pyruvate generation and respiratory metabolism instead of using glucose for antibody glycosylation through the hexosamine biosynthesis pathways[74]. In the gut, Kunisawa et al.[75] also found that IgA$^+$ PC use both the glycolytic pathway and TCA cycle, while naïve B cells in the PP rely on the TCA cycle. By measuring oxygen consumption rate and proton efflux contributed by glycolysis, we found that *Dock8*-deficient IgA$^+$ PCs have reduced respiration.

We propose a model based on our findings and the recent work of others in which the metabolic demands imposed on PCs differ between different niches (e.g. BM and gut), dictating differential lifespans for potentially long-lived PCs. As compared with PCs in the BM, turnover of gut IgA$^+$ PCs is more rapid[35,83,84]. Diurnal changes in intestinal IgA$^+$ PC function and IgA secretion are thought to be driven by changes in nutrient availability because of circadian feeding activity[35]. Thus, IgA$^+$ PC in the LP must adapt to this cyclical metabolic stress. Impaired metabolic fitness of *Dock8*-deficient IgA$^+$ PCs may constrain their ability to adapt to these cyclical changes in nutrient availability in the gut, limiting their survival within the LP. However, *Dock8*-deficient IgA$^+$ PCs persist at other sites, such as the BM, which may present a more stable metabolic environment and is consistent with the known lack of recirculation of IgA$^+$ PCs from the BM to gut despite shared origins[38]. The pattern of antibodies impacted by DOCK8 loss also raises the possibility, which will need to be directly addressed in future studies, that the metabolic requirements of gut PCs might differ between T-dependent and T-independent IgA responses. Altogether, such a model has potential implications for the differential lifespan of antibody production based on T-dependence, isotype (IgGs *vs.* IgA), and location (BM *vs.* gut).

MATERIALS AND METHODS

Mice.

Age and sex-matched 6-to-12-week-old mice were kept on peanut- and egg-free Teklad Global 18% Protein Rodent Diet (2018S, Harlan laboratories). WT CD45.2 and CD45.1 C57BL/6 mice were purchased from the National Cancer Institute. *Dock8* knockout (*Dock8*$^{-/-}$) and *Dock8* flox (*Dock8*$^{fl/fl}$) mice were generated as described previously[23,85]. MuMT$^{-/-}$ [B6.129S2-Ighmtm1Cgn/J], *Cd4-Cre* [Tg(Cd4-cre)1Cwi/BfluJ], and *Cd23-Cre* [B6.Cg-Tg(Fcer2a-cre)5Mbu/J][53] mice purchased from The Jackson Laboratories and *Dock8 flox* mice generated in our lab were crossed to create conditional T cell (T-Dock8$^{-/-}$ mice) and B cell-*Dock8*$^{-/-}$ (B-Dock8$^{-/-}$ mice) knockout mice as per described[39]. The *Dock8-TurboID* knock-in mouse allele was generated using direct delivery of CRISPR-Cas9 reagents to mouse zygotes. A 1kb sequence containing a GSG linker, TurboID, HA tag, and stop codon was introduced in frame into the final exon of *Dock8* (Ensembl Gene ID ENSMUSG00000052085) immediately upstream of the stop codon in exon 48 (Ensembl Dock8–201 transcript ENSMUST00000025831.7). PCR primers flanking the gRNA target site, but outside the repair template homology arms, were used to amplify the 4.5kb region of interest from founder progeny. PCR amplicons were subjected to Sanger sequencing to identify founders with correctly targeted modification. Mice with the correct insertion were backcrossed to C57BL/6J to establish the *Dock8-TurboID* line (see supplementary methods for detailed description). Mice were kept in specific pathogen-free conditions. All protocols

used in this study were approved by the Institutional Animal Care and Use Committee at the Yale University School of Medicine or Northwestern University Feinberg School of Medicine.

Immunization.

Mice were immunized weekly for 6 weeks by oral gavage with 5 mg of ground blanched peanut (Western Mixers Produce & Nuts) or 1 mg of NP-Ovalbumin (LGC Bio-search) with 10 μg CT (List Biologicals, Lot: #10167A2 and #10165A1) in 200 μl of 0.2 M sodium bicarbonate buffer per mouse based on a protocol modified from (10). *E. coli* heatlabile toxin (LT), generously provided by Dr. E. B. Norton, was used in place of CT for some experiments.

Mouse stool processing.

Stool pellets were flash frozen on dry ice upon collection. Frozen pellets were weighed and rehydrated with 1 mL of PBS (Gibco) per 100 mg stool for 15 mins on ice. Rehydrated pellets were homogenized using a sterilized wooden applicator (McKesson), vortexed, and centrifuged at 8000 g for 10 minutes at 4 °C. Supernatant was collected in sterile microcentrifuge tubes, which were pre-coated with 1% Bovine Serum Albumin (BSA) overnight. Supernatant was then stored at −80 °C prior to analysis.

Serum collection.

Collected blood was incubated at RT for 1 hour, and the resulting clot removed. Samples were centrifuged for 10 minutes at 1500 g and the serum was collected and stored at −80 °C prior to analyses.

Enzyme-linked Immunosorbent Assay (ELISA).

Stool and serum samples were analyzed by ELISA for measurement of total, NP-, CT-, or peanut-specific antibodies. Briefly, 20 μg/mL of crude peanut extract (Greer Laboratories; Lot: #287729), 10 μg/mL of NP7/15-BSA (LGC Biosearch), 5 μg/mL CT (List biologicals; Lot: #10165A1 and #10167A2), anti-mouse IgA (MP Biomedicals), anti-mouse IgG (Jackson Laboratories), antimouse IgM, or anti-mouse IgE (BD Pharmingen) capture antibodies in carbonate buffer (pH 9.6) were coated on 96-well Maxisorp plates (Thermo Fisher Scientific) overnight. Plates were blocked with 1% BSA in PBS at 37 °C for 1-hour followed by the addition of serially diluted serum or stool samples with a 2-hour incubation at 37 °C. Peanut-specific, CT-specific, NP-specific, or total IgA were detected with horseradish peroxidase (HRP)-conjugated goat anti-mouse IgA (#1040–05) while total IgG, IgM, and IgE were detected with HRP-conjugated goat anti-mouse IgG (#1013–05) or IgE (#1110–05; Southern Biotech) or HRP-conjugated rat anti-mouse IgM (BD Biosciences #550588) antibodies at 37 °C. For mouse antibodies, purified mouse IgA, IgM, IgE (BD Biosciences), and purified mouse IgG (Sigma-Aldrich) were used as standards. Antigen (Ag)- specific IgA standards were obtained from pooled serum or stool supernatant from hyperimmunized mice. Plates were developed with stabilized chromogen tetramethylbenzidine (Life Sciences) and stopped with 3N hydrochloric acid before reading at 450 nm on a microplate reader (Molecular Devices).

Enzyme-linked immunospot (ELISpot) assay.

96 well ELI-spot multiscreen HTS plates (Merck Millipore) were coated with 20 μg/mL crude peanut extract (Greer Laboratories), 5 μg/mL CT, or anti-mouse IgA (MP Biomedicals) in PBS at 4 °C overnight. Plates were washed with sterile PBS, blocked with complete media (RPMI with 10% fetal bovine serum, 2% penicillin/streptomycin, 2 mM L-glutamine, 25 mM Hepes buffer, and 55 μM β-mercaptoethanol) for 2 h at 37 °C. 1×10^5 cells from the SiLP, 0.5×10^6 cells from the mesenteric lymph nodes (MLN) or Peyer's patches (PP), and 1×10^6 cells from the BM of mice 1 week after 6th intragastric immunizations with peanut and CT were added in triplicates and diluted 1:2 in two serial dilutions. Cells were cultured at 37 °C for 20–22 h. The plates were washed in PBS with 0.01% Tween 20. AP-conjugated goat anti-mouse IgA antibodies (Southern Biotech) were added and incubated for 2 hours at 37 °C. Antibody-forming cells were visualized using blue AP substrate kit (Vector Labs) and quantified using an ImmunoSpot analyzer (Cellular Technology Limited).

Stool IgA Flow Cytometry and Sorting of IgA^+ and IgA^- Bacteria.

IgA sorting and sequencing procedure were performed as in[42]. Briefly, approximately 100 mg of stool pellets were incubated with 1 mL of sterile PBS (Gibco) for 30 minutes before homogenization in Fast Prep Lysing Matrix D tubes containing ceramic beads (MP Biomedicals) on a bead beater mini homogenizer for 7 seconds. Centrifugation was carried out at 50 *g* for 15 minutes at 4 °C to remove large particles. 100 μL of supernatant containing stool bacteria were removed and washed with 1 mL of staining buffer (PBS containing 1% (w/v) Bovine Serum Albumin (BSA, American Bio) before centrifugation at 8000 *g* for 5 minutes at 4 °C (washing step) and resuspension in 1 mL of staining buffer. A pre-sort sample (30 μL) was collected and frozen at −80 °C before 16S rRNA sequencing. After an additional wash, bacterial pellets were resuspended in 100 μL blocking buffer (staining buffer with 20% Normal Rat Serum (Stem cell technologies)) on ice for 20 minutes before staining on ice for 30 minutes with 100 μL of staining buffer containing 1:12.5 dilution of PE-conjugated Rat anti-mouse IgA (eBioscience clone mA-6E1). Samples were then washed 3 times with 1 ml staining buffer before flow cytometric analysis or Fluorescence Activated Cell Sorting (FACSAria; BD Biosciences) to separate the IgA^+ and IgA^- bacteria. For each sample, 2 million IgA^+ and IgA^- bacteria were collected.

16S rRNA sequencing and statistical analyses.

Frozen bacterial samples were resuspended in 400 μL staining buffer before adding 250 μL 0.1 mm zirconia/silica beads (Biospec), 300 μL Lysis buffer (200 mM NaCl, 200 mM Tris, 20 mM EDTA, pH 8), 200 μL 20% SDS, and 500 μL phenol:chloroform:isoamyl alcohol (25:24:1, pH 7.9; Sigma). After incubation on ice for 4 minutes, bacterial cells were homogenized by 2 rounds of bead beating with 2 minutes of incubation on ice in between before centrifugation at 6000 *g* at 4 °C. Aqueous phase was transferred to a Phase Lock Gel tube (Light; 5 PRIME) before an equal volume of phenol:chloroform:isoamyl alcohol was added. Samples were mixed before centrifugation at 16,100 *g* for 3 minutes at room temperature. DNA precipitation was performed using 1/10 volume of 3 M NaOAc (pH5.5) and 1 volume Isopropanol to the aqueous phase before overnight incubation at 20 °C. DNA

precipitate was pelleted at 16,100 g for 20 minutes at 4 °C before washing in 500 μL of absolute EtOH, centrifugation was performed 16,100 *g* for 3 minutes at 4 °C before DNA pellet was for 15 minutes with no heat (miVac GeneVac on Auto Run setting). Lastly, DNA pellet was resuspended in 100 μL of TE buffer (pH 7) and incubated at 50 °C for 30 min. 35 U/ml RNase A was added to the DNA pellet before purification and elution in 40 μL Elution Buffer (QIAquick PCR purification; QIAGEN). 16S rRNA sequencing of the V4 region and bacterial genome sequencing were performed on an Illumina miSeq using barcoded primers. For detailed protocol on sequencing, refer to supplementary information in[42]. Analyses of 16S sequencing data were performed using QIIME (version 1.9.1)[86]

All the samples were rarefied to 20,000 reads. We identified the contaminant OTUs in control water samples and removed them from all the analysis using filter_otus_from_otu_table.py script, prepared taxa summaries, alpha- and beta-diversity tables, and principal coordinate analysis (PCoA) using summarize_taxa.py, alpha_diversity.py, and beta_diversity_through_pl ots.py. Principle coordinate analyses were prepared in R v.3.3.2 (R Core Team (2016). R: A language and environment for statistical computing. R Foundation for Statistical Computing, Vienna, Austria. URL https://www.R-project.org/). Cladogram was prepared using FigTree v1.4.3 http://tree.bio.ed.ac.uk/software/figtree/. LefSe analysis was performed on platform provided by the Huttenhower lab as described in [43].

16S rRNA sequence data availability.

All sequence read data have been deposited with links to BioProject accession number GSE198847 in the NCBI BioProject database (https://www.ncbi.nlm.nih.gov/bioproject/)

SFB IgA flow.

To generate SFB without IgA coating, Stools from SFB-monocolonized mice (gifted by Dr. Ivaylo Ivanov) were orally transferred into germ-free *Rag*$^{-/-}$ mice. 5 days later, stools were collected from *Rag*$^{-/-}$ mice and homogenized. Large particles were removed by centrifuge, and remaining SFB were washed as described in “Stool IgA Flow Cytometry and Sorting of IgA^{+} and IgA^{-} Bacteria” section. SFB were then incubated with 1:10 diluted stool supernatants from WT and *Dock8*$^{-/-}$ mice in the presence of 1% rat serum for 1 hour on ice. As a control for non-specific binding of IgA to SFB, stool supernatants from mice freshly purchased from SFB-free facility, The Jackson Laboratories, were incubated with isolated SFB to establish a baseline for background IgA staining. After wash, SFB pellets were blocked with 20% rat serum for 20 minutes on ice, then stained with 1:50 dilute of APC-conjugated Rat anti-mouse IgA (eBioscience #17-4204-82), 1:200 diluted SYTO9 nucleic acid stain (Invitrogen #S34854), and 5 μg/ml DAPI (Sigma #D9542). Flow cytometry was used to identify the percentage of IgA-coating SFB.

LP cell isolation.

The protocol used to isolate cells from the LP varied over the course of this work as these preps are challenging and often resulted in loss of all viable cells. The protocol that we find works the best is described here. All steps were performed using RPMI media supplemented with 1% Penicillin and Streptomycin, 1% L-glutamine, 25 mM Hepes, 1X non-essential

amino acids, 1X Sodium Pyruvate, and 50 μM of β-mercaptoethanol (“Serum-free RPMI”). Additional reagents were added to the media at specific steps noted below.

Following harvest, the small intestine was removed by cutting 1 mm from the stomach and 1 mm above the cecum. PPs were removed and stored in RPMI with 10% FBS for processing. The small bowel was cut open longitudinally for removal of fecal matter through repeated washing in Hanks balanced salt solution. While processing subsequent samples, the cleaned intestine was stored in RPMI with 10% FBS on ice. After cleaning, each small bowel was cut into 1–2 cm pieces and placed into a conical flask containing room-temperature Serum-free RPMI with added 3% FBS, 5 mM EDTA, and 0.145 mg/ml of Dithiothreitol. The samples were stirred at 600 rpm at 37 °C in an incubator with 5% CO2 for 20 mins. The small intestine pieces were then washed thrice with 30 seconds of vigorous shaking in Serum-free RPMI with 2 mM EDTA. Between each wash, the media was washed through a strainer and discarded along with the epithelial and intra-epithelial lymphocyte fraction, while the remaining intestine pieces were collected into new media. A final wash was performed using room-temperature Serum-free RPMI with no additives and samples were washed through a new strainer. Subsequently, the small intestine was cut into fine pieces before incubation with stirring, in the same conditions as previous step, in 10 mL of serum-free RPMI media with 1 mg/mL Collagenase IV (Worthington Biochemical #LS004189) and 0.05% DNase I (Sigma-Aldrich #D5025). After 30 minutes of digestion, the reaction was stopped with 10 mL cold Serum-free RPMI with 3% FBS. The sample was then ground through a 70 μM cell strainer with the plunger of a 3 mL syringe before centrifugation at 1500 rpm. The pellet was then resuspended and filtered again through a 40 μM cell strainer before centrifugation at 1500 rpm. Enrichment of lymphocytes was performed through separation of cells using a 30% percoll gradient. Centrifugation was performed at 2000 rpm (Acceleration: 4, Deceleration: 2 at 20 ° C). The resulting pellet contains LP lymphocytes. Occasionally, there will be visible red blood cells as well, in which case, RBC lysis should be performed before any further analysis. Further staining of lymphocytes from the LP fraction is performed in FACS Buffer (PBS+ 2% FBS 1 mM EDTA) at room temperature for 20 minutes to avoid overstaining. Use of Collagenase IV limits surface marker digestion, so both surface and intracellular staining are possible following this protocol.

Cellular analyses by flow cytometry.

Peanut-immunized mice were sacrificed 8 days after the 6th oral dose of peanut and CT. LP cells were isolated as described above. PP, MLN, and spleen were harvested, homogenized, and the cells were washed and resuspended in 2% Fetal Bovine Serum in Phosphate Buffered Saline before being incubated with fluorochrome-conjugated antibody cocktail for 30 min on ice. Anti-mouse B220 (RA3–6B2), CD19 (6D5), CD21/35 (7E9), CD23 (B3B4), GL7 (GL7), IgD (11–26c.2a), CD138 (281–2), CD40 (3/23), CCR9 (CW-1.2), and α4β7 (DATK32) antibodies were purchased from Biolegend. Anti-mouse IgG1 (A85–1), CD69 (H1.2F3), CD95 (Jo2), and CD16/32 (2.4G2) antibodies were purchased from BD Biosciences. Anti-mouse IgA (mA-6E1), Ki67 (SolA15) antibodies, and LIVE/DEAD™ Fixable Aqua Dead Cell Stain Kit were purchased from Thermo Fisher Scientific. Phospho-Stat3 (Tyr 705) (D3A7) was purchased from Cell Signaling Technology. IgA, IgD, Ki67, and CD138 were stained intracellular in fixed and permeabilized cells using BD Fixation/

Permeabilization Solution Kit (BD Biosciences) according to manufacturer's instruction. All flow cytometry samples were scanned on BD FACS LSRII (BD Biosciences) or MACSQuant (Miltenyi) flow cytometers and analyzed by FlowJo software (Version 9.3.2, TreeStar).

NP-conjugation and antigen-specific B cells staining.

NP-conjugation method was adapted from previous report[87]. Briefly, R-PE (Anaspec AS-82004), APC (AAT Bioquest 2554), and PerCP (AAT Bioquest 2559) were diluted with distilled H_2O to 10 mg/ ml and dialyzed against H_2O, followed by 0.05M $NaHCO_3$ buffer. NP-Osu (Biosearch Technologies N-1010-100) was added to the protein solutions in a 20:1 molar ratio and mixed at room temperature for 12 hours. The conjugated proteins were then dialyzed against 0.05M NaHCO3 buffer, followed by PBS. NP-conjugates staining was performed intracellularly at 10 nM for 1–2 hours with other antibodies.

Microscopy.

MLN and PP from B-Dock8$^{-/-}$ and littermate controls were snap frozen in a cryomold with O.C.T. Compound (Tissue-Tek, Sakura) and stored at −80 °C. Tissues were cut into 6-μm sections and processed as described previously[88]. Briefly, frozen sections were rehydrated with plain PBS before blocking with 10% rat serum 1% BSA 0.1% Tween-20, PBS solution. Slides were stained with the following antibodies: anti-mouse B220 (RA3–6B2), CD11c (N418), TCRβ (H57–597), and IgA (mA-6E1). The images were acquired immediately after staining with the Nikon eclipse Ti microscope using 4x or 10x objectives. Affinity photo software (Serif) was used for image analysis.

Mixed BM chimeras.

Recipient WT CD45.1$^+$ mice were irradiated with two doses of 600 rad 3 hours apart. One hour after the second irradiation, 5×10^5 BM cells from WT (CD45.1.2$^+$) or *Dock8*$^{-/-}$ (CD45.1.2$^+$) mice mixed with 5×10^5 BM cells from MuMT$^{-/-}$ (Ighm$^{-/-}$) mice were adoptively transferred by i.v. injection into irradiated naïve WT recipient mice. All experiments with BM chimeric mice were performed 8–12 weeks after BM transplant.

Immunoblotting.

Splenic B cells were sorted on FACS Aria (BD Biosciences) based on CD23 and CD19 expression. One million cells were lysed in immunoprecipitation assay buffer with protease inhibitors (Roche), and cell lysates were run on SDS–PAGE and transferred onto nitrocellulose membrane. After blocking with 5% non-fat milk in Tris-buffered saline with 0.1% Tween-20 for 1 hour at room temperature, the membrane was incubated with anti-mouse DOCK8 antibody (Takara) at 4 °C overnight. 1:5000 goat anti-rabbit IgG(H+L)-HRP polyclonal detection antibody (Invitrogen) was incubated with membrane before assessing chemiluminescence signal with ECL substrate on chemidoc imager (Biorad). Housekeeping protein β-Actin was used for normalizing protein concentration.

In vivo CT challenge

Mice were immunized with 10 μg of CT in 200 μL bicarbonate buffer for weekly for 2 weeks. 10–14 days after the last immunization, mice were fasted for 12 hours prior to intragastric challenge with 20 μg CT in 200 μL bicarbonate buffer. 12 hours after challenge, mice were sacrificed and weighed before and after removal of small intestine to assess weight of small intestine. Cecum weight was measured by removing cecum from small intestine. Intestinal fluid accumulated in cecum was released from punctured cecum, and volume of fluid recovered was measured.

In vitro IgA$^+$ B cell cultures.

BM cells were cultured in complete RPMI media with 10% homemade Flt3L for 10 days to induce DC differentiation according to this protocol[89]. Naïve B cells from spleen or PP were isolated using B cell isolation kit (STEMCELL Technologies #19854) with 0.8 μg/ml biotin anti-CD43 antibodies (BD 553269). Naïve B cells were then cultured with BMDCs in a 1:1 ratio in the presence of 0.5 μg/ml CD40L (R&D 8230-CL-050), 10 μg/ml anti-IgM (Jackson ImmunoResearch 115-006-020), 2 ng/ml TGFβ (PeproTech 100–21), and 100 nM RA (Sigma R2625) for 4–5 days to induce IgA switching and PC differentiation.

Transwell assays.

IgA$^+$ B cells were isolated from MLN of Ctrl and B-Dock8$^{-/-}$ mice by FACS and labeled with CFSE or CTV, respectively. Cells from Ctrl and B-Dock8$^{-/-}$ mice with different labels were mixed in a 1:1 ratio and loaded in the upper wells of 96-well Transwell plates (Corning 3385). 250 nM CCL25 (Biolegend 589302) in complete media was added in the bottom wells. Cells were cultured at 37C incubator with CO_2 for 2 hours to allow migration. The number of IgA$^+$CCR9$^+$ B cells in bottom and upper wells were then counted and assessed by flow cytometry. The percentages of migrated cells were calculated as number in bottom wells/(number in bottom well + number in upper well).

Collagen gel migration assays.

Collagen gel matrix was prepared using PuroCol (Advanced BioMatrix 7626) and Nutragen (Advanced BioMatrix 7774) in 1X EMEM (Lonza 12–684F) and 0.4% sodium bicarbonate, then diluted with complete RPMI media to 1.5 mg/ml and 3 mg/ml, respectively. The matrix containing CCL25 (250 nM) was loaded into chambers and left to polymerize at 37 °C for 1 hour. *In vitro* switched IgA B cells from WT and *Dock8*$^{-/-}$ were labeled with CFSE or CTV, respectively, and loaded on the top of collagen gel. Cells were cultured at 37 °C with CO_2 overnight to allow migration. The chambers were visualized using Leica 6000 microscope, and the migration distances of cells were measured using ImageJ.

TurboID protein isolation.

Naïve B cells from PP of WT and *Dock8-TurboID* knock-in mice were cultured in *in vitro* IgA switching condition as mentioned before. 5 days later, biotin was added to the culture media to a final concentration of 50 μM and was incubated in a 37 °C incubator with CO_2 for 3 hours. Cells were then harvested, and live IgA$^+$ B cells were sorted by FACS. Sorted cells were resuspended in lysis buffer containing 50 mM Tris-Hcl, 500 mM

NaCl, 0.2% SDS, 1 mM DTT, 2% Triton X-100, and 1X complete protease inhibitor (Roche 11836170001) and sonicated. The cell lysis was centrifuged at 16,500 g for 10 minutes to remove cell debris. The supernatants were mixed with magnetic streptavidin beads (Invitrogen #65001) overnight at 4 °C. The samples were then put on a magnetic rack. The supernatants were removed, and magnetic beads were washed with 2% SDS. The beads were then washed with a buffer containing 0.1% deoxycholic acid, 1% Triton X-100, 1 mM EDTA, 500 mM NaCl, and 50 mM HEPES, followed by a buffer containing 0.5% deoxycholic acid, 0.5% NP-40, 1 mM EDTA, 250 mM LiCl, and 10 mM Tris-HCl.

TurboID mass spectrometry sample preparation.

After the final wash in the TurboID affinity purification protocol, an additional wash was performed using 500 μL of 50 mM ammonium bicarbonate, pH 8.2. A magnet was applied, the supernatant removed, and protein-bound bead samples were resuspended in 100 μL of proteolytic digestion buffer (50 mM ammonium bicarbonate, pH 8.2). Note that this resuspension in the proteolytic digestion buffer is essential if freezing the bound beads as that process diminishes the bead integrity and supernatant cannot be removed after freezing. Resuspended samples were flash frozen and shipped overnight to The Jackson Laboratory Mass Spectrometry and Protein Chemistry Service on dry ice. Dithiothreitol was added to a final concentration of 10 mM and incubated at 42 °C for 30 minutes on a thermomixer set to 850 rpm (adjust as necessary to keep the beads from settling). Samples were cooled to room temperature, and iodoacetamide was added to a final concentration of 20 mM for alkylation. Samples were then incubated in the dark at 25 °C on a thermomixer set to 850 rpm (adjust as necessary to keep beads from settling) for 30 minutes. Following alkylation, 500 ng of sequence grade modified trypsin (Promega, #V511A) were added to each sample and incubated for 16 h (overnight) at 37 °C on a thermomixer set to 850 rpm to avoid bead settling (adjust as necessary to keep beads from settling). After 16 h, 100 ng of sequence grade modified trypsin was added, and samples were incubated for another 4 h at 37 °C on a thermomixer set to 850 rpm. Proteolytic digestion was then quenched by adding 1% TFA to each sample (check to make sure the pH is between 3–4 and adjust as necessary). Quenched samples were then cleaned using Millipore C18 zip-tips (#ZTC18S096) according to manufacturer protocol. While following the C18 zip-tip manufacturer protocol, the wetting solution was 100% acetonitrile, the equilibration and wash solutions were 0.1% TFA, and the elution was 60% acetonitrile with 0.1% TFA. All peptide eluents were then dried down in a vacuum centrifuge for 20 mins or until dry.

TurboID Liquid Chromatography Tandem Mass Spectrometry (LC-MS/MS) Analysis.

Dried peptide samples were reconstituted in 25 μL of 98% H2O/2% acetonitrile/0.1% formic acid by pipetting liquid on the sides of the tubes a minimum of ten times, vortexing for 30 seconds, and then incubating 10 mins at 700 rpm on a thermomixer at 22 °C. Following reconstitution, the samples were centrifuged for 30 seconds on a table-top low speed centrifuge. The supernatant was then transferred to a mass spectrometry vial and put at 4 °C in the Ultimate 3000 autosampler. Samples were then analyzed using a Thermo Eclipse Tribrid Orbitrap mass spectrometer with a FAIMS Pro interface coupled to a nano-flow UltiMate 3000 liquid chromatography system in the Mass Spectrometry and Protein Chemistry Service at The Jackson Laboratory. The method duration was run at a flow rate of

300 nL/min with a 150 mins gradient of Buffer A (100% H2O with 0.1% formic acid) and Buffer B (100% acetonitrile with 0.1% formic acid) with a 30 mins equilibration using 98% A/2% B included (180 minutes total). The Eclipse Tribrid Orbitrap global parameter settings included peptide mode, a default charge state of 2, expected peak width of 30 seconds, and advance peak determination. The instrument method consisted of two nodes that were identical but with different FAIMS voltages; these voltages consisted of −40 V and −50 V. For the precursor spectra detection (MS1) in each node, the settings included: cycle time = 1 second (each node), detector = orbitrap, orbitrap resolution = 240,000, scan range = 375–1200 m/z, RF lens % = 40, normalize AGC target (%) = 250, maximum inject time (ms) = auto, microscans = 1, data type = profile, polarity = positive, monoisotopic precursor selection = peptide, charge states = 2–7, dynamic exclusion of a n = 1 for 60 seconds, and a minimum intensity threshold of 5^{e+03}. Peptide fragment analysis (MS2) settings included: quadrupole isolation mode, isolation window (m/z) = 0.7, collision energy (%) = 33 (fixed), activation type = HCD, detector type = ion trap, ion trap scan rate = turbo, maximum inject time = 35 ms, microscans = 1, and data type = centroid.

TurboID Mass Spectrometry Data Analysis and Statistical Comparisons.

The RAW mass spectrometry files were searched and compared using Proteome Discoverer (version 2.5.0.400) in the Mass Spectrometry and Protein Chemistry Service at The Jackson Laboratory. During the processing workflow in Proteome Discoverer, individual Thermo .RAW files were searched against the *Mus musculus* database (sp_tr_incl_isoforms TaxID = 10090) (v2021-02-04) using Sequest HT. Search parameters included trypsin digest, precursor mass tolerance of 10 ppm, fragment mass tolerance of 0.6 Da, carbamidomethyl on cysteines (+57.021 Da) and oxidation of methionine (+15.995 Da) as a dynamic modification, acetylation of the amino-terminus (+42.011 Da) as a dynamic modification, a maximum number of missed cleavages of two, minimum peptide length = 6, and maximum peptide length = 144. In the Percolator node in the workflow the target/decoy selection = concatenated, validation was based on q-value, the maximum delta Cn = 0.05, and a false discovery rate <0.05 for all matches. Minora feature detector parameters were set to Thermo recommended defaults. Multiple comparisons between the TurboID and control samples were then performed using the consensus workflow feature in Proteome Discoverer on all identified peptide spectra. Precursor spectra abundances were based on intensity and were normalized to total peptide amount scaled on average, with maximum fold change of 100 allowed for ratio calculations. Protein abundance calculations used summed abundances, protein ratios were protein abundance based, low abundance resampling imputation was utilized, and a background-based t test was performed on identified targets in the comparisons. An FDR < 0.05 filter and strict parsimony principle were applied to protein matches within the dataset for comparison. Additional pathway analysis was performed using IPA (QIAGEN) and GO analysis using g:Profiler[90].

PLA.

Naïve B cells from spleens of WT and *Dock8-TurboID* knock-in mice were cultured in *in vitro* IgA switching condition as described above. After 4 days cells were harvested and seeded onto Poly-L-Lysine-coated coverslips (Corning) and allowed to adhere for 30 mins at 37 °C. Coverslips were rinsed with PBS, and cells fixed with 4%PFA in PBS for 10 minutes

at room temperature before washing 3 times with PBS. Cells were permeabilized with 0.1% Triton X-100 in PBS for 10 minutes at room temperature before washing 3 times with PBS. PLA was performed using the Duolink® In Situ Red kit (Millipore Sigma) following the manufactures instructions. The following antibodies were used: anti-PKM antibody (Abcam – ab150377 – 1:50 dilution) and anti-HA tag antibody (Abcam – ab49969 – 1:500 dilution). PLA antibody staining was performed at 4 °C overnight. Images were acquired on a Nikon A1R confocal microscope, and data were analyzed using Imaris software. Nuclei and PLA spots were counted in 3D volume images in Imaris using automatic spot detection to avoid bias of manual detection.

Glycolytic Rate Assay.

Naïve B cells were isolated from spleens of WT and *Dock8*$^{-/-}$ mice. After stimulation with CD40L, F(ab')2 anti-IgM, TGFβ, BMDCs, and RA for 5 days, cells were collected for seahorse assay. Activated B cells were seeded at 500,000 per well in Seahorse XF cell culture plates pre-coated with Cell-Tak. Cells were rested in RPMI base medium pH 7.4, supplemented with 2 mM L-glutamine, 1 mM sodium pyruvate, and 10 mM glucose in a non-CO2 incubator for 45 min prior the assay. Glycolytic rate was assessed using the Seahorse XF Glycolytic Rate Assay kit (Agilent). Data acquisition was performed on a Seahorse XF96 Extracellular Flux Analyzer (Agilent).

Statistical Analyses.

All statistical analyses except IgA-Seq and proteomics data were performed using GraphPad Prism software. Data were analyzed with Mann-Whitney U test (two experimental groups) or Kruskal-Wallis test (three experimental groups or more) followed by Dunn's test for post-hoc analyses. Statistical significance is defined as *$p < 0.05$, **$p < 0.01$, and ***$p < 0.001$. IgA-Seq data analyses were as described above.

Supplementary Material

Refer to Web version on PubMed Central for supplementary material.

ACKNOWLEDGMENTS

We would like to thank M. Firla and J. Goldstein for technical assistance as well as J. S. Chen, S. Olyha, D. Liu, J. Anthonypillai, T. A. Rice, L. W. Wang, D. Bhattacharya, J. Gommerman, O. Rojas, and W. Khoury-Hanold for helpful discussion and review of this manuscript. We would also like to acknowledge the Mass Spectrometry and Protein Chemistry Service at The Jackson Laboratory for their contribution to the mass spectrometry work performed in this study. We are grateful to Dr. Ivaylo Ivanov for sharing of his SFB-monocolonized mice and expertise with us. We gratefully acknowledge the contribution of Rebecca Boumil and the Genetic Engineering Technologies Service at The Jackson Laboratory for expert assistance with the work described in this publication.

FUNDING

This study was supported by Ira & Diana Riklis Family Research Award in Food Allergy, Food Allergy Research & Education (FARE), a grant from the Food Allergy Science Initiative, Inc., R01 AI136942 (to S.C.E.), R56 AI155497 (to S.C.E.), the National Science Scholarship from the Agency for Science, Technology, and Research, Singapore (to B.Z.), and the China Scholarship Council-Yale World Scholars Fellowship (to S.C.). Mass spectrometry analysis was performed on a Thermo Eclipse Tribrid Orbitrap obtained through a National Institutes of Health S10 award (1 S10 OD026816-;01). The authors declare no competing financial interests.

References

1. Chen K, Magri G, Grasset EK & Cerutti A. Rethinking mucosal antibody responses: IgM, IgG and IgD join IgA. Nat. Rev. Immunol 20, 427–441 (2020). [PubMed: 32015473]
2. Sutherland DB, Suzuki K. & Fagarasan S. Fostering of advanced mutualism with gut microbiota by immunoglobulin A. Immunol. Rev 270, 20–31 (2016). [PubMed: 26864102]
3. Conrey PE et al. IgA deficiency destabilizes homeostasis toward intestinal microbes and increases systemic immune dysregulation. Sci. Immunol 8, eade2335 (2023).
4. Lycke N. & Holmgren J. Long-term cholera antitoxin memory in the gut can be triggered to antibody formation associated with protection within hours of an oral challenge immunization. Scand. J. Immunol 25, 407–412 (1987). [PubMed: 3576134]
5. Elson CO & Ealding W. Generalized systemic and mucosal immunity in mice after mucosal stimulation with cholera toxin. J. Immunol 132, 2736–2741 (1984). [PubMed: 6233359]
6. Corthésy B. Multi-faceted functions of secretory IgA at mucosal surfaces. Front. Immunol 4, 185 (2013). [PubMed: 23874333]
7. Berin MC Mucosal antibodies in the regulation of tolerance and allergy to foods. Semin. Immunopathol 34, 633–642 (2012). [PubMed: 22777546]
8. Pabst O. & Slack E. IgA and the intestinal microbiota: the importance of being specific. Mucosal Immunol. 13, 12–21 (2020). [PubMed: 31740744]
9. Liu EG et al. Food-specific immunoglobulin A does not correlate with natural tolerance to peanut or egg allergens. Sci. Transl. Med 14, eabq0599 (2022).
10. Hand TW & Reboldi A. Production and function of immunoglobulin A. Annu. Rev. Immunol 39, 695–718 (2021). [PubMed: 33646857]
11. Bergqvist P, Gärdby E, Stensson A, Bemark M. & Lycke NY Gut IgA class switch recombination in the absence of CD40 does not occur in the lamina propria and is independent of germinal centers. J. Immunol 177, 7772–7783 (2006). [PubMed: 17114448]
12. Zhang B. et al. Divergent T follicular helper cell requirement for IgA and IgE production to peanut during allergic sensitization. Sci. Immunol 5, eaay2754 (2020).
13. Castigli E. et al. TACI and BAFF-R mediate isotype switching in B cells. J. Exp. Med 201, 35–39 (2005). [PubMed: 15630136]
14. Varfolomeev E. et al. APRIL-deficient mice have normal immune system development. Mol. Cell. Biol 24, 997–1006 (2004). [PubMed: 14729948]
15. Grasset EK et al. Gut T cell–independent IgA responses to commensal bacteria require engagement of the TACI receptor on B cells. Sci. Immunol 5, eaat7117 (2020).
16. Borsutzky S, Cazac BB, Roes J. & Guzmán CA TGF-β receptor signaling is critical for mucosal IgA responses. J. Immunol 173, 3305–3309 (2004). [PubMed: 15322193]
17. Cazac BB & Roes J. TGF-beta receptor controls B cell responsiveness and induction of IgA in vivo. Immunity 13, 443–451 (2000). [PubMed: 11070163]
18. Côté JF & Vuori K. GEF what? Dock180 and related proteins help Rac to polarize cells in new ways. Trends Cell Biol. 17, 383–393 (2007). [PubMed: 17765544]
19. Meller N, Merlot S. & Guda C. CZH proteins: a new family of Rho-GEFs. J. Cell Sci 118, 4937–4946 (2005). [PubMed: 16254241]
20. Su HC Dedicator of cytokinesis 8 (DOCK8) deficiency. Curr Opin Allergy Clin. Immunol 10, 515–520 (2011).
21. Zhang Q. et al. Combined immunodeficiency associated with *DOCK8* mutations. N. Engl. J. Med 361, 2046–2055 (2009). [PubMed: 19776401]
22. Schneider C. et al. Migration-induced cell shattering due to DOCK8 deficiency causes a type 2–biased helper T cell response. Nat. Immunol 21, 1528–1539 (2020). [PubMed: 33020661]
23. Krishnaswamy JK et al. Migratory CD11b+ conventional dendritic cells induce T follicular helper cell-dependent antibody responses. Sci. Immunol 2, eaam9169 (2017).
24. Krishnaswamy JK et al. Coincidental loss of DOCK8 function in NLRP10-deficient and C3H/HeJ mice results in defective dendritic cell migration. Proc. Natl Acad. Sci. U. S. A 112, 3056–3061 (2015). [PubMed: 25713392]

25. Harada Y. et al. DOCK8 is a Cdc42 activator critical for interstitial dendritic cell migration during immune responses. Blood 119, 4451–4461 (2012). [PubMed: 22461490]
26. Zhang Q. et al. DOCK8 regulates lymphocyte shape integrity for skin antiviral immunity. J. Exp. Med 211, 2549–2566 (2014). [PubMed: 25422492]
27. Singh AK et al. DOCK8 regulates fitness and function of regulatory T cells through modulation of IL-2 signaling. JCI Insight 2, e94275 (2017).
28. Jabara HH et al. DOCK8 functions as an adaptor that links TLR-MyD88 signaling to B cell activation. Nat. Immunol 13, 612–620 (2012). [PubMed: 22581261]
29. Sun X. et al. Dock8 regulates BCR signaling and activation of memory B cells via WASP and CD19. Blood Adv. 2, 401–413 (2018). [PubMed: 29472447]
30. Randall KL et al. Dock8 mutations cripple B cell immunological synapses, germinal centers and long-lived antibody production. Nat. Immunol 10, 1283–1291 (2009). [PubMed: 19898472]
31. Kunimura K. et al. S100A4 protein is essential for the development of mature microfold cells in Peyer's patches. Cell Rep. 29, 2823–2834.e7 (2019). [PubMed: 31775048]
32. Engelhardt KR et al. The extended clinical phenotype of 64 patients with dedicator of cytokinesis 8 deficiency. J. Allergy Clin. Immunol 136, 402–412 (2015). [PubMed: 25724123]
33. Engelhardt KR et al. Large deletions and point mutations involving the dedicator of cytokinesis 8 (DOCK8) in the autosomal-recessive form of hyper-IgE syndrome. J. Allergy Clin. Immunol 124, 1289–1302.e4 (2009). [PubMed: 20004785]
34. Gatz SA et al. Curative treatment of autosomal-recessive hyper-IgE syndrome by hematopoietic cell transplantation. Bone Marrow Transplant. 46, 552–556 (2011). [PubMed: 20622910]
35. Penny HA et al. Rhythmicity of intestinal IgA responses confers oscillatory commensal microbiota mutualism. Sci. Immunol 7, eabk2541 (2022).
36. Mei HE et al. Blood-borne human plasma cells in steady state are derived from mucosal immune responses. Blood 113, 2461–2469 (2009). [PubMed: 18987362]
37. Lemke A. et al. Long-lived plasma cells are generated in mucosal immune responses and contribute to the bone marrow plasma cell pool in mice. Mucosal Immunol. 9, 83–97 (2016). [PubMed: 25943272]
38. Wilmore JR et al. IgA plasma cells are long-lived residents of gut and bone marrow that express isotype- and tissue-specific gene expression patterns. Front. Immunol 12:791095.
39. Gowthaman U. et al. Identification of a T follicular helper cell subset that drives anaphylactic IgE. Science 365, eaaw6433 (2019).
40. Kawamoto S. et al. Foxp3+ T cells regulate immunoglobulin A selection and facilitate diversification of bacterial species responsible for immune homeostasis. Immunity 41, 152–165 (2014). [PubMed: 25017466]
41. Gutzeit C, Magri G. & Cerutti A. Intestinal IgA production and its role in host-microbe interaction. Immunol. Rev 260, 76–85 (2014). [PubMed: 24942683]
42. Palm NW et al. Immunoglobulin A coating identifies colitogenic bacteria in inflammatory bowel disease. Cell 158, 1000–1010 (2014). [PubMed: 25171403]
43. Segata N. et al. Metagenomic biomarker discovery and explanation. Genome Biol. 12, R60 (2011). [PubMed: 21702898]
44. Clements JD, Hartzog NM & Lyon FL Adjuvant activity of Escherichia coli heat-labile enterotoxin and effect on the induction of oral tolerance in mice to unrelated protein antigens. Vaccine 6, 269–277 (1988). [PubMed: 3048010]
45. Clements JD & Norton EB The mucosal vaccine adjuvant LT(R192G/L211A) or dmLT. mSphere 3. e00215–18.
46. Hornqvist E. & Lycke N. Defense against cholera toxin is strongly CD4+ T cell dependent. Infect. Immun 59, 3630–3638 (1991). [PubMed: 1910010]
47. Tokuhara D. et al. Secretory IgA-mediated protection against V. cholerae and heat-labile enterotoxin-producing enterotoxigenic Escherichia coli by rice-based vaccine. Proc. Natl Acad. Sci. U. S. A 107, 8794–8799 (2010). [PubMed: 20421480]

48. Lycke N, Erlandsson L, Ekman L, Schön K. & Leanderson T. Lack of J Chain inhibits the transport of gut IgA and abrogates the development of intestinal antitoxic protection. J. Immunol 163, 913–919 (1999). [PubMed: 10395687]
49. Tangye SG et al. Dedicator of cytokinesis 8–deficient CD4 + T cells are biased to a T H 2 effector fate at the expense of T H 1 and T H 17 cells. J. Allergy Clin. Immunol 139, 933–949 (2017). [PubMed: 27554822]
50. Janssen E. et al. DOCK8 enforces immunological tolerance by promoting IL-2 signaling and immune synapse formation in Tregs. JCI Insight 2, e94298 (2017).
51. Tsuji M. et al. Preferential generation of follicular B Helper T cells from Foxp3+ T cells in gut Peyer's patches. Science 323, 1488–1492 (2009). [PubMed: 19286559]
52. Hirota K. et al. Plasticity of TH17 cells in Peyer's patches is responsible for the induction of T cell–dependent IgA responses. Nat. Immunol 14, 372–379 (2013). [PubMed: 23475182]
53. Kwon K. et al. Instructive role of the transcription factor E2A in early B lymphopoiesis and germinal center B cell development. Immunity 28, 751–762 (2008). [PubMed: 18538592]
54. Liu D. et al. IL-10-dependent crosstalk between murine marginal zone B cells, macrophages, and CD8α+ dendritic cells promotes Listeria monocytogenes. Infect. Immun 51, 64–76.e7 (2019).
55. Palm A-K-E & Kleinau S. Marginal zone B cells: from housekeeping function to autoimmunity? J. Autoimmun 119.
56. Reboldi A. et al. IgA production requires B cell interaction with subepithelial dendritic cells in Peyers patches. Science 352, aaf4822 (2016).
57. Macpherson AJ, McCoy KD, Johansen FE & Brandtzaeg P. The immune geography of IgA induction and function. Mucosal Immunol. 1, 11–22 (2008). [PubMed: 19079156]
58. Mora JR et al. Generation of gut-homing IgA-secreting B cells by intestinal dendritic cells. Science 314, 1157–1160 (2006). [PubMed: 17110582]
59. Berlin C. et al. Alpha 4 beta 7 lntegrin Mediates lymphocyte Binding to the Mucosal Vascular addressin MAdCAM-1. Cell 74, 185–195 (1993). [PubMed: 7687523]
60. Kunisawa J. et al. Microbe-dependent CD11b+ IgA+ plasma cells mediate robust early-phase intestinal IgA responses in mice. Nat. Commun 4, 1772 (2013). [PubMed: 23612313]
61. Isho B, Florescu A, Wang AA & Gommerman JL Fantastic IgA plasma cells and where to find them. Immunol. Rev 303, 119–137 (2021). [PubMed: 34046908]
62. Lamm ME & Phillips-Quagliata JM Origin and homing of intestinal IgA antibody-secreting cells. J. Exp. Med 195, F5–F8 (2002). [PubMed: 11805155]
63. Craig SW & Cebra JJ Peyer's patches: an enriched source of precursors for IgA-producing immunocytes in rabbit. J. Exp. Med 134, 188–200 (1971). [PubMed: 4934147]
64. Keles S. et al. Dedicator of cytokinesis 8 regulates signal transducer and activator of transcription 3 activation and promotes T H 17 cell differentiation. J. Allergy Clin. Immunol 138, 1384–1394.e2 (2016). [PubMed: 27350570]
65. Linterman MA et al. IL-21 acts directly on B cells to regulate Bcl-6 expression and germinal center responses. J. Exp. Med 207, 353–363 (2010). [PubMed: 20142429]
66. Zotos D. et al. IL-21 regulates germinal center B cell differentiation and proliferation through a B cell–intrinsic mechanism. J. Exp. Med 207, 365–378 (2010). [PubMed: 20142430]
67. Avery DT et al. B cell–intrinsic signaling through IL-21 receptor and STAT3 is required for establishing long-lived antibody responses in humans. J. Exp. Med 207, 155–171 (2010). [PubMed: 20048285]
68. Bryant VL et al. Cytokine-mediated regulation of human B cell differentiation into Ig-secreting cells: predominant role of IL-21 produced by CXCR5+ T follicular helper cells. J. Immunol 179, 8180–8190 (2007). [PubMed: 18056361]
69. Ding BB, Bi E, Chen H, Yu JJ & Ye BH IL-21 and CD40L synergistically promote plasma cell differentiation through upregulation of Blimp-1 in human B cells. J. Immunol 190, 1827–1836 (2013). [PubMed: 23325890]
70. Cao AT et al. Interleukin (IL)-21 promotes intestinal IgA response to microbiota. Mucosal Immunol. 8, 1072–1082 (2015). [PubMed: 25586558]

71. Cho H. et al. Defective IgA response to atypical intestinal commensals in IL-21 receptor deficiency reshapes immune cell homeostasis and mucosal immunity. Mucosal Immunol. 12, 85–96 (2019). [PubMed: 30087442]
72. Branon TC et al. Efficient proximity labeling in living cells and organisms with TurboID. Nat. Biotechnol 36, 880–887 (2018). [PubMed: 30125270]
73. Ripperger TJ & Bhattacharya D. Transcriptional and metabolic control of memory B cells and plasma cells. Annu. Rev. Immunol 39, 345–368 (2021). [PubMed: 33556247]
74. Lam WY et al. Mitochondrial pyruvate import promotes long-term survival of antibody-secreting plasma cells. Immunity 45, 60–73 (2016). [PubMed: 27396958]
75. Kunisawa J. et al. Mode of bioenergetic metabolism during B cell differentiation in the intestine determines the distinct requirement for vitamin B 1. Cell Rep. 13, 122–131 (2015). [PubMed: 26411688]
76. Bunker JJ et al. Innate and adaptive humoral responses coat distinct commensal bacteria with immunoglobulin A. Immunity 43, 541–553 (2015). [PubMed: 26320660]
77. Suzuki K. et al. Aberrant expansion of segmented filamentous bacteria in IgA-deficient gut. Proc. Natl Acad. Sci. U. S. A 101, 1981–1986 (2004). [PubMed: 14766966]
78. Cong Y, Feng T, Fujihashi K, Schoeb TR & Elson CO A dominant, coordinated T regulatory cell-IgA response to the intestinal microbiota. Proc. Natl Acad. Sci. U. S. A 106, 19256–19261 (2009). [PubMed: 19889972]
79. Cao AT, Yao S, Gong B, Elson CO & Cong YT Th17 Cells upregulate polymeric Ig receptor and intestinal IgA and contribute to intestinal homeostasis. J. Immunol 189, 4666–4673 (2012). [PubMed: 22993206]
80. Berin MC & Wang W. Reduced severity of peanut-induced anaphylaxis in TLR9-deficient mice is associated with selective defects in humoral immunity. Mucosal Immunol. 6, 114–121 (2013). [PubMed: 22718261]
81. Kim D. et al. Nod2-mediated recognition of the microbiota is critical for mucosal adjuvant activity of cholera toxin. Nat. Med 22, 524–530 (2016). [PubMed: 27064448]
82. Bowman EP et al. The intestinal chemokine thymus-expressed chemokine (CCL25) attracts IgA antibody-secreting cells. J. Exp. Med 195, 269–275 (2002). [PubMed: 11805153]
83. Koike T. et al. Progressive differentiation toward the long-lived plasma cell compartment in the bone marrow. J. Exp. Med 220, e20221717 (2023).
84. Hapfelmeier S. et al. Reversible microbial colonization of Germ-free mice reveals the dynamics of IgA immune responses. Science 328, 1705–1709 (2010). [PubMed: 20576892]
85. Calabro S. et al. Bridging channel dendritic cells induce immunity to transfused red blood cells. J. Exp. Med 213, 887–896 (2016). [PubMed: 27185856]
86. Caporaso JG et al. QIIME allows analysis of high-throughput community sequencing data. Nat. Methods 7, 335–336 (2010). [PubMed: 20383131]
87. Komban RJ et al. Activated Peyer^{0}s patch B cells sample antigen directly from M cells in the subepithelial dome. Nat. Commun 10, 2423 (2019). [PubMed: 31160559]
88. Calabro S. et al. Differential intrasplenic migration of dendritic cell subsets tailors adaptive immunity. Cell Rep. 16, 2472–2485 (2016). [PubMed: 27545885]
89. Naik SH et al. Cutting edge: generation of splenic CD8+ and CD8− dendritic cell equivalents in Fms-like tyrosine kinase 3 ligand bone marrow cultures. J. Immunol 174, 6592–6597 (2005). [PubMed: 15905497]
90. Raudvere U. et al. g:profiler: a web server for functional enrichment analysis and conversions of gene lists (2019 update). Nucleic Acids Res. 47, W191–W198 (2019). [PubMed: 31066453]

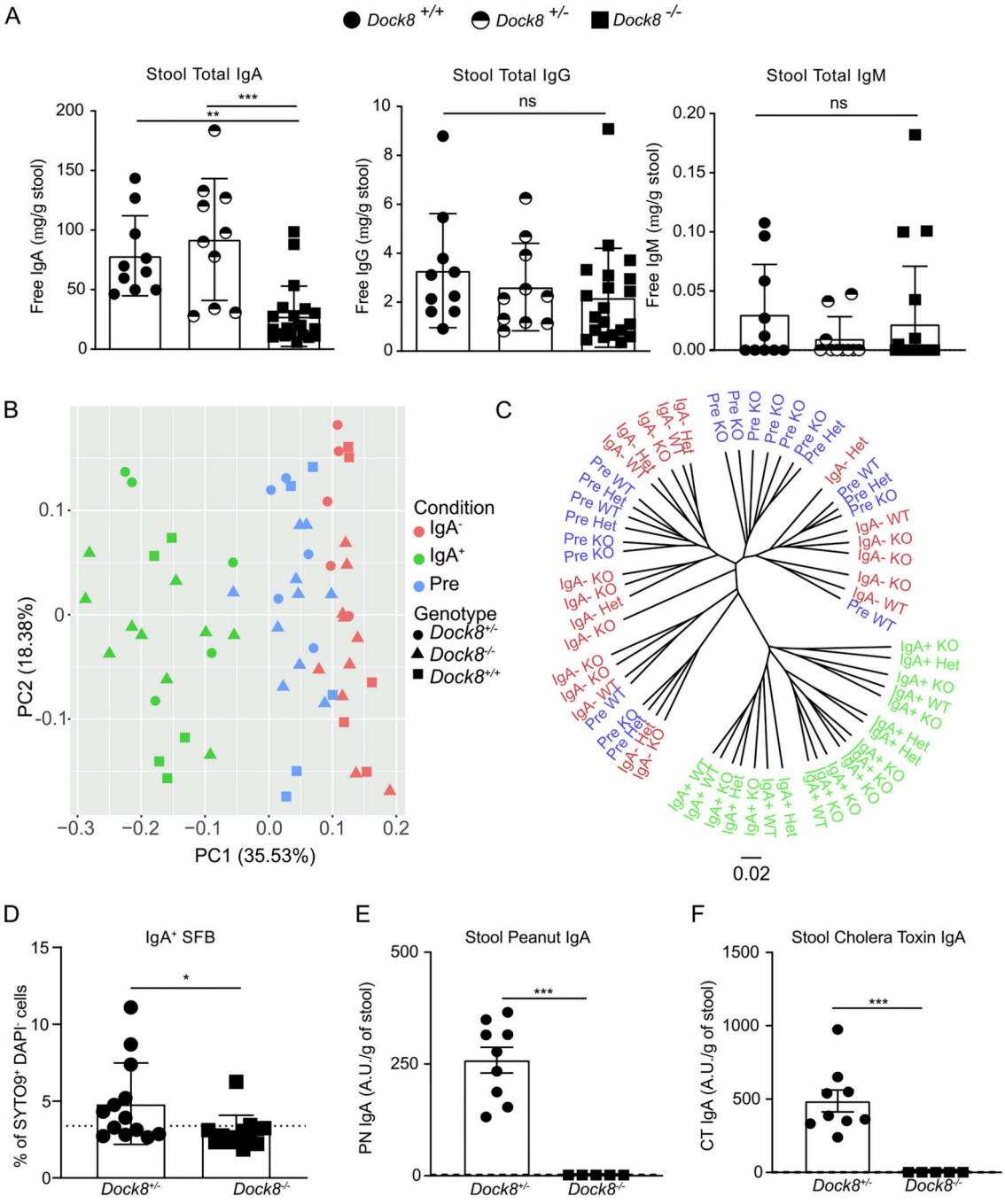

Fig. 1. *Dock8*-deficient mice have impaired IgA production to a wide array of antigenic targets in the gut.

ELISA quantification of (A) total stool IgA, IgG, and IgM in WT (*Dock8*$^{+/+}$; closed circles), *Dock8* heterozygous (Dock8$^{+/-}$; half-filled circles), and *Dock8* knockout (*Dock8*$^{-/-}$; closed squares) cohoused littermates at steady state. (B) Principal coordinate analysis (PCoA) and (C) cladogram of weighted UniFrac distances of total (presort), sorted IgA^{+} and IgA^{-} fecal bacteria from *Dock8*$^{+/+}$, *Dock8*$^{+/-}$, or *Dock8*$^{-/-}$ mice. Scale range: 0.02. (D) Frequency of IgA binding of segmented-filamentous bacteria (SFB) isolated from fecal pellets of SFB

mono-colonized mice and then incubated with fecal supernatant from *Dock8*$^{+/-}$ or *Dock8*$^{-/-}$ cohoused littermates. Dotted line indicates frequency of IgA binding of SFB incubated with fecal supernatant from WT mice raised in SFB-free facility. ELISA quantification of (E) stool peanut-specific IgA and (F) stool cholera toxin (CT)-specific IgA in *Dock8*$^{+/+}$, *Dock8*$^{+/-}$, and *Dock8*$^{-/-}$ cohoused littermates one week after the 6th weekly intragastric (i.g.) immunization with peanut and CT. Dotted lines indicate detection limit of 1.56 arbitrary units. (A, E-F) Data are representative of 3 independent experiments with 4–10 *Dock8*$^{+/+}$, 4–10 *Dock8*$^{+/-}$, and 4–20 *Dock8*$^{-/-}$ mice. (B-C) Data are representative of two independent experiments with 5–10 mice per group. (D) Pooled data from 2 independent experiments with 5–8 mice per group. Statistical tests: (A) Kruskal-Wallis analysis and Dunn's post-hoc (D-F) Mann-Whitney U test, whereby $*P < 0.05$, $**P < 0.01$, $***P < 0.001$, ns = not significant, and nd = not detectable, respectively. Error bars indicate SD; each symbol represents an individual mouse.

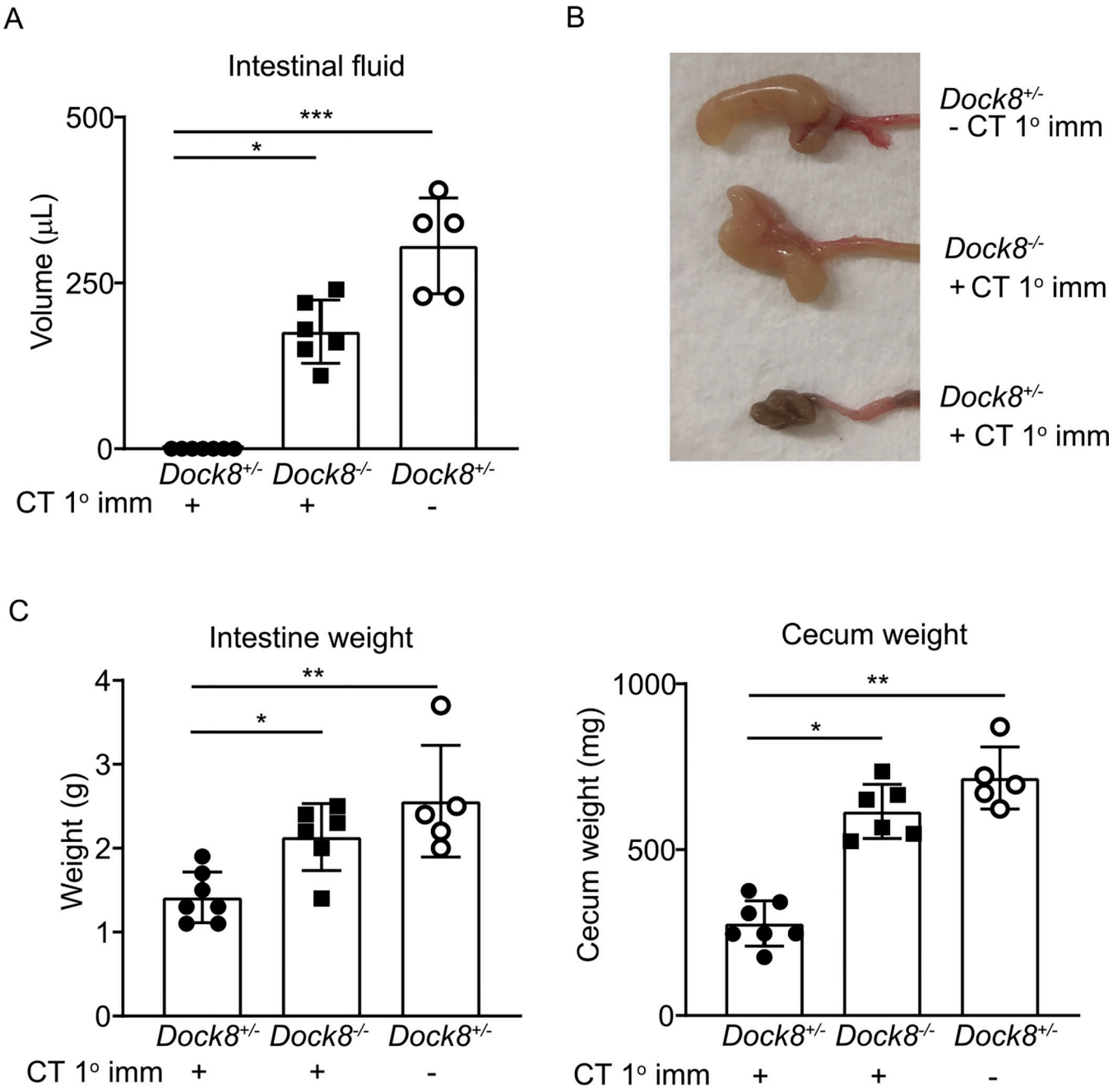

Fig. 2. Loss of T-dependent IgA in the absence of DOCK8 impairs intestinal protection from toxins.

(A) Quantification of intestinal fluid accumulation (B) representative images of fluid accumulation in cecum and quantification of (C) small intestine weight or (D) cecum weight of mice 12 hours after oral CT challenge in naïve *Dock8*$^{+/-}$ mice (CT 1° imm -) or CT-immunized (CT 1° imm +) *Dock8*$^{+/-}$ and *Dock8*$^{-/-}$ cohoused littermates. CT-immunized mice received 2 weekly CT i.g. and were challenged 10–14 days later. Statistical tests: (A, C-D) Kruskal-Wallis analysis with Dunn's posthoc test, whereby *$P < 0.05$, **$P < 0.01$,

***$P < 0.001$, ns = not significant. Error bars indicate SD. (A-D) Pooled data from 2 independent experiments with 3–4 mice per group.

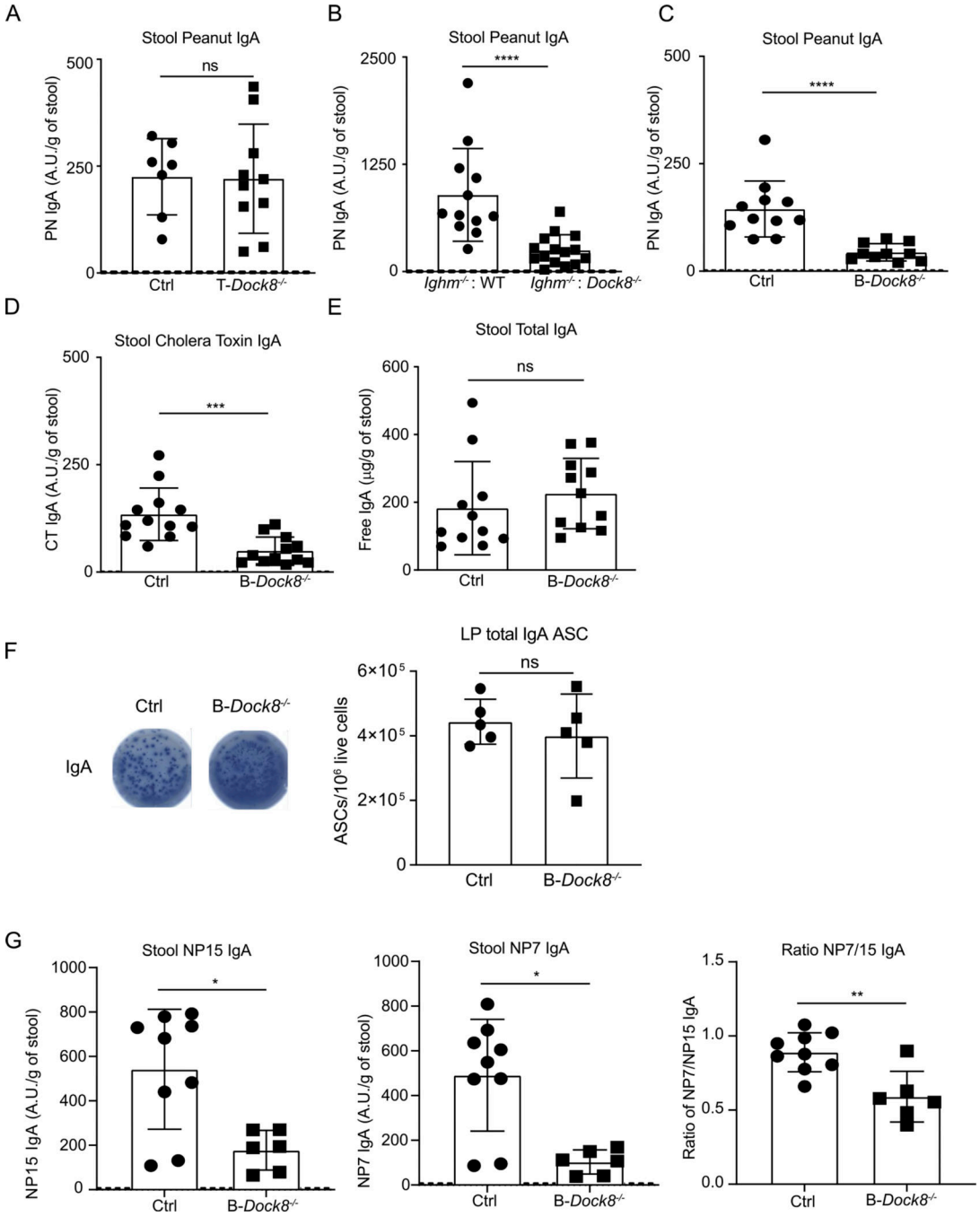

Fig. 3. B cell-intrinsic *Dock8* deficiency impairs gut IgA production to T-dependent antigens.

ELISA quantification of stool peanut-specific IgA in mice immunized orally with peanut and CT: (A) cohoused Ctrl (*Dock8*$^{flox/flox}$) and T-Dock8$^{-/-}$ (*Cd4*^{cre}*Dock8*$^{flox/flox}$) littermates (B) cohoused irradiated mice reconstituted with 1:1 mixture of B cell-deficient muMt (*Ighm*$^{-/-}$) and wild-type (WT) or *Dock8*-deficient (*Dock8*$^{-/-}$) bone marrow cells, or (C) cohoused Ctrl (*Dock8*$^{flox/flox}$) and B-Dock8$^{-/-}$ (*Cd23*^{cre}*Dock8*$^{flox/flox}$) littermates. (D) ELISA quantification of stool CT-specific IgA in peanut/CT immunized cohoused Ctrl (*Dock8*$^{flox/flox}$) and B-Dock8$^{-/-}$ (*Cd23*^{cre}*Dock8*$^{flox/flox}$) littermates. Peanut and CT-specific

IgA are measured one week after the 6th weekly i.g. immunizations with peanut and CT. (E) ELISA quantification of total stool IgA from immunized cohoused Ctrl and B-Dock8$^{-/-}$ littermates. (F) Representative images and enumeration of IgA-secreting cells (ASCs) by ELISpot in the small intestine LP (SiLP) from Ctrl and B-Dock8$^{-/-}$ cohoused littermates. (G) ELISA quantification of stool NP15-specific, NP7-specific, and ratio of NP7/NP15 IgA in cohoused Ctrl (*Dock8*$^{flox/flox}$) and B-Dock8$^{-/-}$ littermates one week after the 6th weekly i.g. immunizations with NP19-OVA and CT. Dotted lines indicate the detection limit of the CT IgA, peanut IgA, and NP7 and NP15 IgA assay at 1.56 arbitrary units relative to standard. Statistical tests: (A-G) Mann-Whitney U test, whereby *$P < 0.05$, **$P < 0.01$, ***$P < 0.001$, **** < 0.000, ns = not significant. Error bars indicate SD. (A-G) Pooled data from 2–3 independent experiments with 3–5 mice per group. Lamina propria preparation with low number of viable cells is excluded from analyses in (F).

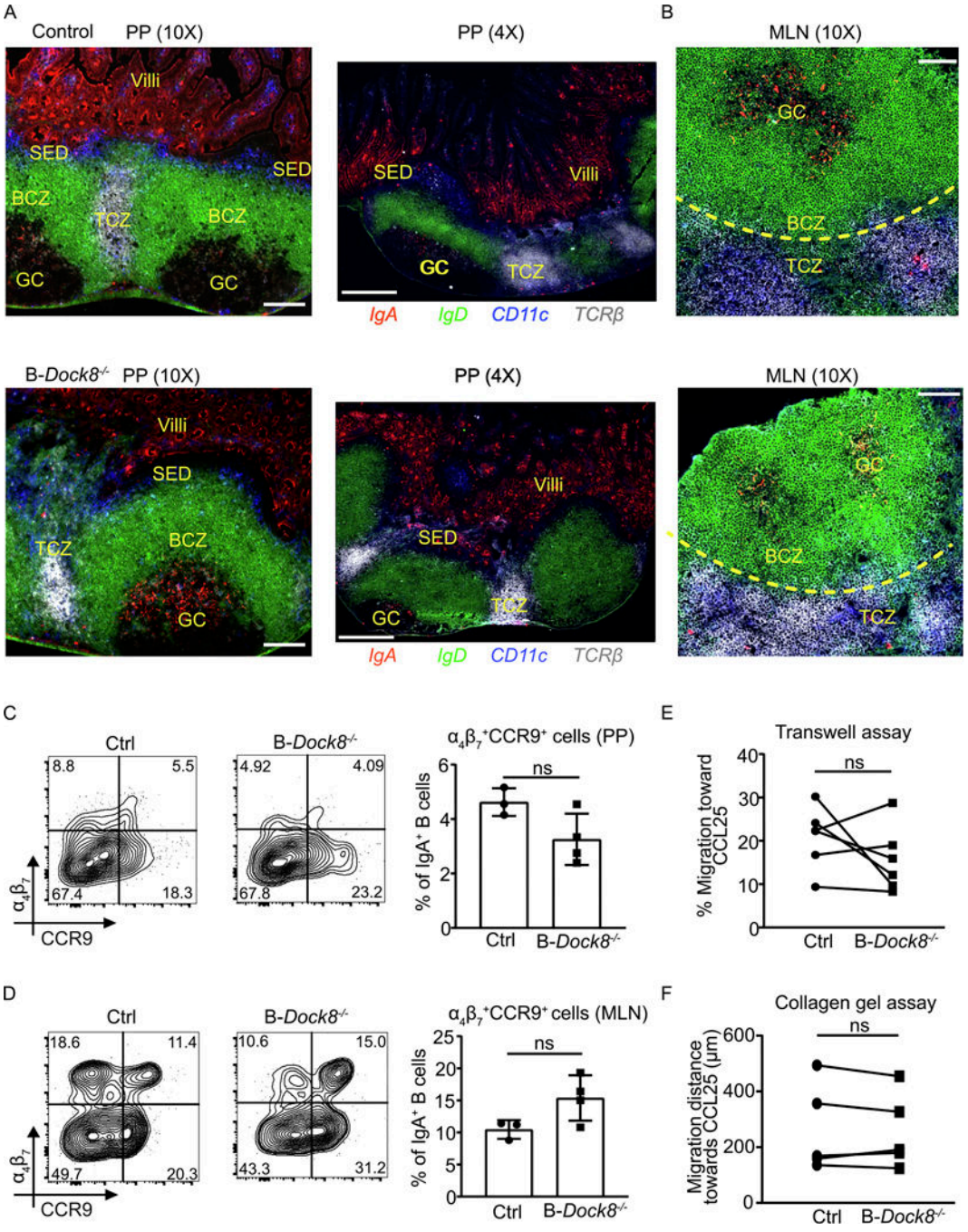

Fig. 4. B cell-intrinsic *Dock8* deficiency does not alter B cell migration, gut homing, or MLN and PP architecture.

Representative immunofluorescent images depicting localization of TCRβ$^+$ (white), IgD$^+$ (green), IgA$^+$ (red), or CD11c$^+$ (blue) cells in (A) PP or (B) MLN at steady state in Ctrl and B-Dock8$^{-/-}$ cohoused littermates. GC = germinal centers, SED = subepithelial dome, TCZ = T cell zone, and dotted lines demarcates BCZ = B cell zone. Scale bars, 100 μm for 10x images and 4x images. (C-D) Representative flow cytometry plots and frequency of surface CCR9$^+$ and α β $^+$ cells among live IgA$^+$ B cells in (C) PP and (D) MLN in cohoused Ctrl (*Dock8$^{flox/flox}$*) and B-Dock8$^{-/-}$ littermates. (E) Transwell migration assay

of Ctrl and *Dock8*-deficient IgA^+ $CCR9^+$ B cells towards CCL25. (F) Quantification of migration distance of Ctrl and *Dock8*-deficient *in vitro* differentiated IgA^+ B cells within 3D collagen gel towards CCL25. Statistical tests: (C-D) Mann-Whitney U test or (E-F) Paired t test; ns = not significant. Error bars indicate SD. (A) Representative images from 3 independent experiments with 3 mice per group. (C-D) Representative data from 2 independent experiments with 3–5 mice per group. (E-F) Combined data from 2 independent experiments.

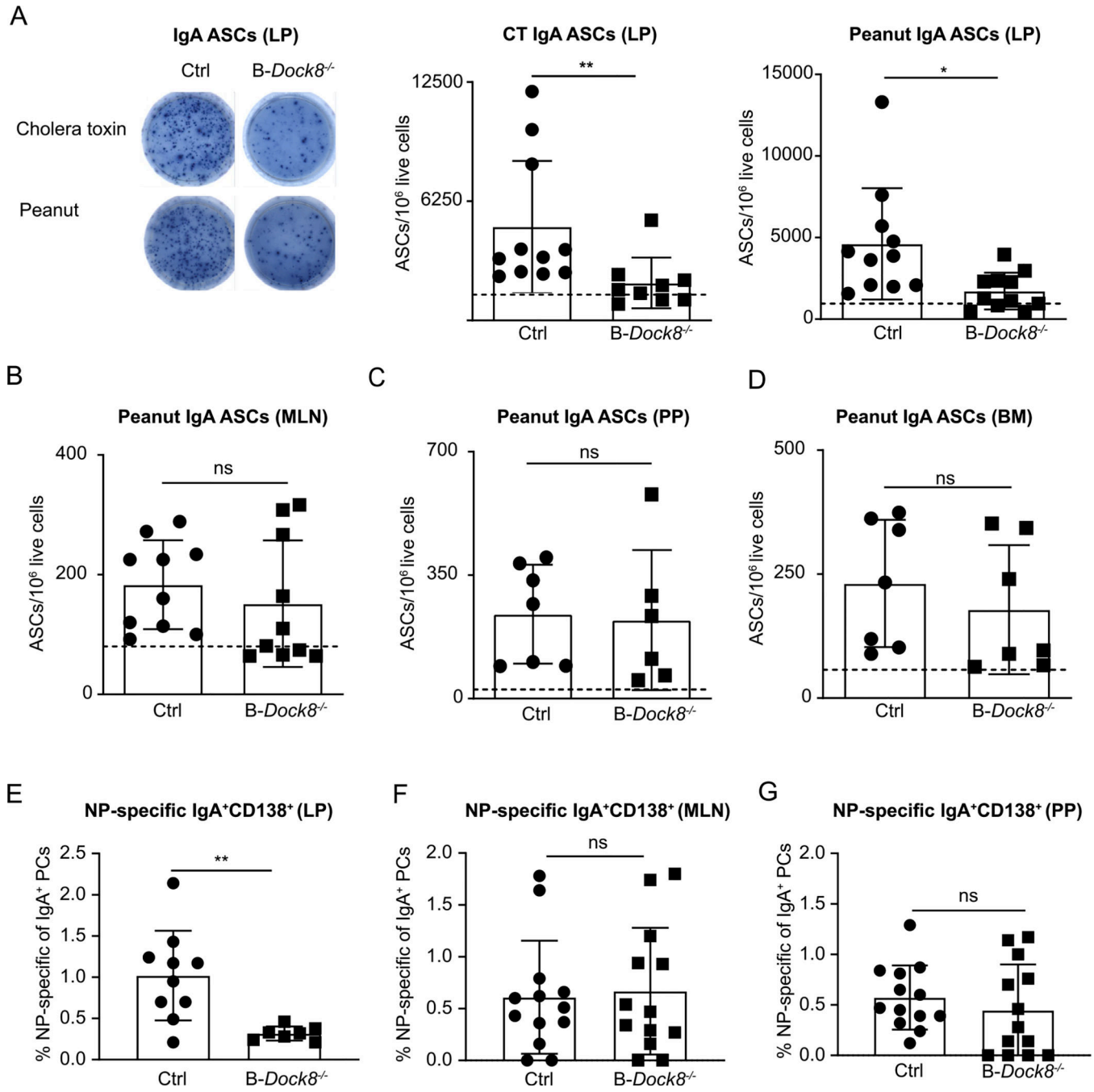

Fig. 5. B cell-intrinsic *Dock8* deficiency results in decreased antigen-specific IgA$^+$ PCs in lamina propria but not PP, MLN, or bone marrow (BM).

(A) Representative images with quantitation of CT-specific and peanut-specific IgA antibody-secreting cells (ASCs) by ELISpot in the small intestine lamina propria (LP). (B-D) Numbers of peanut-specific IgA ASCs in the (B) MLN and (C) PP (D) BM from Ctrl and B-Dock8$^{-/-}$ cohoused littermates. (E) Frequency of NP-specific IgA$^+$CD138$^+$ PCs in LP pre-gated on CD19$^-$Lin$^-$ (NK1.1$^-$ CD3$^-$ TCRβ$^-$ F4/80$^-$ IgD$^-$) cells. (F-G) Frequency of NP-specific IgA$^+$CD138$^+$ PCs pre-gated on live cells in (F) MLN and (G) PP of Ctrl and B-Dock8$^{-/-}$ cohoused littermates. All tissues were analyzed 8 days after 6th weekly

i.g. immunizations with (A-D) peanut+CT or (E-G) NP19-OVA+CT. Statistical tests: Mann-Whitney U test, whereby *$P < 0.05$, **$P < 0.01$, and ns = not significant. Error bars indicate SD. (A-B) Pooled data from 3 independent experiments with 3–4 mice per group. (C-D) Pooled data from 2 independent experiments with 2–3 mice per group. (E-G) Pooled data from 3 independent experiments with 3–5 mice per group. Lamina propria preparation with low number of viable cells is excluded from analyses in (E). Dotted lines represent baseline signal of CT-specific or peanut-specific IgA ASC in naïve mice.

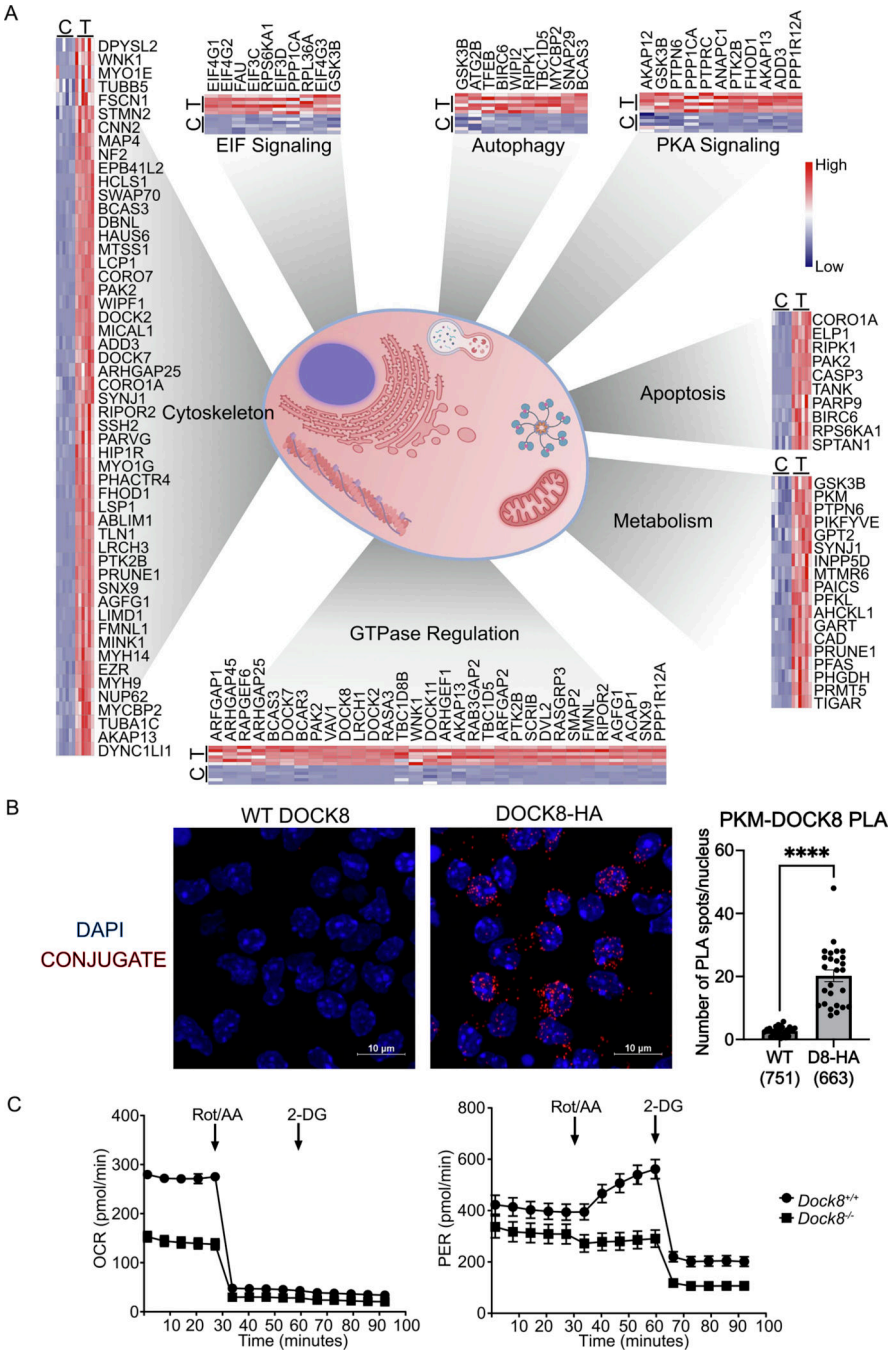

Fig. 6. DOCK8 interactome in IgA$^+$B cells and metabolic assays demonstrate an important role for DOCK8 in IgA B cell respiration.

(A) IgA$^+$ B cells were generated from PPs of DOCK8-TurboID mice as in Fig. S5E. Heatmap of enriched proteins proximal to DOCK8 from proteomics analysis of biotinylated targets. Selected proteins were grouped into functional classes based on gene ontology and IPA analysis. (B) Proximity ligation assay (PLA) showing protein-protein interactions between Pyruvate kinase M1/2 (PKM) and DOCK8 in B cells from IgA$^+$ B cell cultures. Representative images from PLA experiments of wild-type (WT DOCK8) and DOCK8-TurboID (DOCK8-HA) cells (left) and quantification of the number of PLA spots per cell

(right). Data were pooled data from 2 independent experiments and numbers in parentheses indicate the number of individual nuclei scored for each genotype. Error bars indicate SEM. (C) Representative plots of oxygen consumption rate (OCR) and glycolysis proton efflux rate (glycoPER) of in vitro generated IgA^+ B cells from Ctrl and *Dock8*-deficient mice. Data are representative of 2 independent experiments.